UNIVERSITY OF BUCHAREST
VIRTUTE ET SAPIENTIA

FACULTY OF CHEMISTRY

MSc. Thesis

Master student: MIHAI BORDEIAŞU

Thesis Advisor:

Assist. Prof. DELIA-LAURA POPESCU, PhD

2021

FACULTY OF CHEMISTRY

DEPARTAMENT OF INORGANIC CHEMISTRY

MSc. Thesis

Cu(II)-based Metal-Organic Frameworks with Kagomé Layers

Master: Chemistry of Advanced Materials

Master student: MIHAI BORDEIAŞU

Thesis Advisor:

Assist. Prof. DELIA-LAURA POPESCU, PhD

June – July, 2021

Contents

Introduction

Modern society faces great climate changes that affect both the environment and the everyday lifestyle of individuals. One of the main issues is the greenhouse effect exerted by different gases generated from human activity, most notably from burning of fossil fuels, production and transport of coal, natural gas, and oil, during treatment of wastewater as well as from livestock and agricultural practices. Of the greenhouse gases, carbon dioxide (CO_2), methane (CH_4), nitrous oxide (N_2O), and fluorinated gases such as hydrofluorocarbons (HFCs), perfluorocarbons (PFCs), sulfur hexafluoride (SF_6), and nitrogen trifluoride (NF_3) have the most pronounced effect, according to the United States Environmental Protection Agency (EPA). CO_2 is the most abundant, representing approximately 76% of the total greenhouse gases [1].

Studies have shown that for the 1959–2019 period, 19% of the total CO_2 emissions were caused by land-use change while the rest of 81% came from fossil emissions. Global fossil CO_2 emissions have increased every decade, from an average 11 billion tons CO_2 per year in 1960s to an average of 35 billion tons CO_2 per year during 2010–2019, with a maximum of 36.44 billion tons in 2019. The annual fossil CO_2 emissions during this period are presented in Figure 1. In contrast, CO_2 emissions from land use, land-use change, and forestry have remained relatively constant, at around 5 billion tons/year over the past half-century [2]. In 2020, the values decreased, reaching approximately 34 billion tons from fossil emissions, while for land-use change emissions it reached 5.8 billion tons [1].
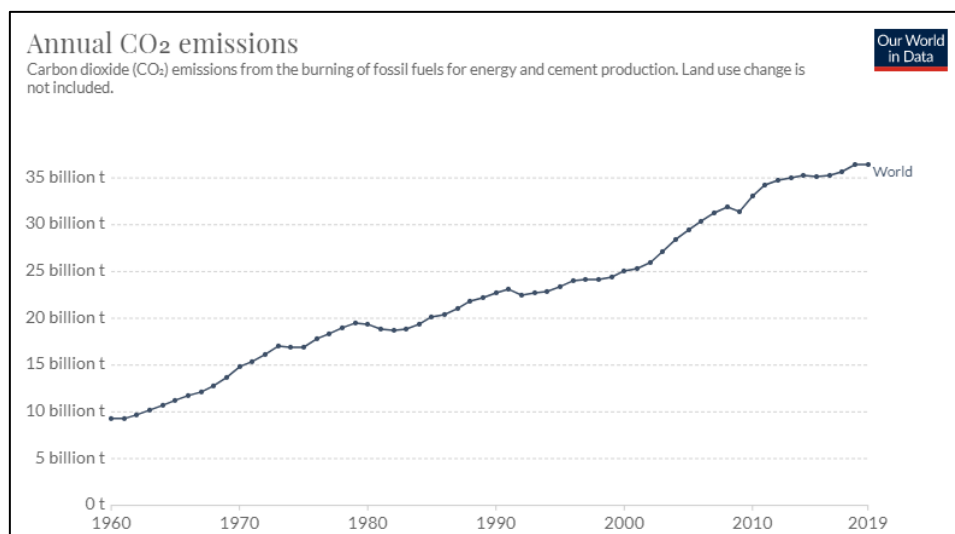

Fig.1. Annual fossil CO_2 emissions during 1960–2019
Source: https://ourworldindata.org

To overcome the large amount of greenhouse gases emitted into the atmosphere, old technologies have been updated and new methods are being developed to decrease the amount produced during certain processes.

For CO_2 capture and storage, different physical, chemical and even biological methods of sequestration have been implemented. The ocean and geological storage [3], as well as direct mineral carbonation [4] are among the most used methods. The storage relies on the injection of carbon dioxide into the ocean, at depths higher than 1000 meters and into porous rock formations, while the mineral carbonation aims to create stable carbonates such as magnesite ($MgCO_3$) and calcite ($CaCO_3$). Biological methods focus around phytoplankton and microalgae which utilizes dissolved CO_2 in photosynthesis for generation of storage carbon sugars [5]. Besides these approaches, carbon dioxide can also be used as raw material in the synthesis of new compounds such as porous coordination polymers, were it would be fixed as carbonate linking different metal ions into an extended structure [6].

The present dissertation focus on the synthesis of Cu-based porous coordination polymers with different bipyridine-based ligands through direct fixation of atmospheric carbon dioxide into the structure and the characterization of the obtained compounds through the use of single-crystal and powder X-ray diffraction, along with spectroscopic techniques, such as FTIR and UV-Vis in solid state.

Our main aim is to obtain a series of compounds that would combine both physical and chemical methods for carbon dioxide sequestration: the chemical fixation into the structure and furthermore, the physical adsorption of carbon dioxide into the pores of the obtained coordination polymers.

The thesis is structured into two main chapters, the former presenting a general overview of porous coordination polymers, their structural features and physical properties, as well as their applications in the fields of catalysis, gas storage and ion exchange. The second chapter comprises the experimental results of the research and is divided into three parts: the synthesis of Cu-based coordination polymers, their structural and spectral characterization, where some unique features are revealed, and the possible applications of these compounds in gas storage and anion-exchanges.

Chapter I. Theoretical Aspects

I.1. Porous Coordination Polymers

Porous coordination polymers (PCPs), most commonly known as Metal-Organic Frameworks (MOFs), are a class of porous materials formed by self-assembly of metal ions or clusters and bridging ligands, whether it is an organic or organometallic ligand, or a coordinative compound with free coordination sites, yielding to an infinite structure characterized by high regularity, tunable pore sizes, large surface area and adjustable internal surface properties [7-9].

A great advantage of these compounds is their diversity as there can be obtained a large variety of coordination polymers depending on the nature of the building blocks and their properties which have a major impact on PCPs topology, defining the final structure. Thus, PCPs may be tuned for a targeted application from the synthesis stage.

Due to their structural characteristics, which lead to versatile architectures, porous coordination polymers are used in different applications (Figure I.1-1.), such as adsorption, separation and storage of gases, heterogeneous catalysis, drug delivery and sensor technology, magnetism, luminescence, water treatment, production of composite resins and fuel cells [10,11]. As a result, the number of published articles related to MOFs has increased greatly in the last 20 years, reaching almost 8000 publications in 2019 [11].
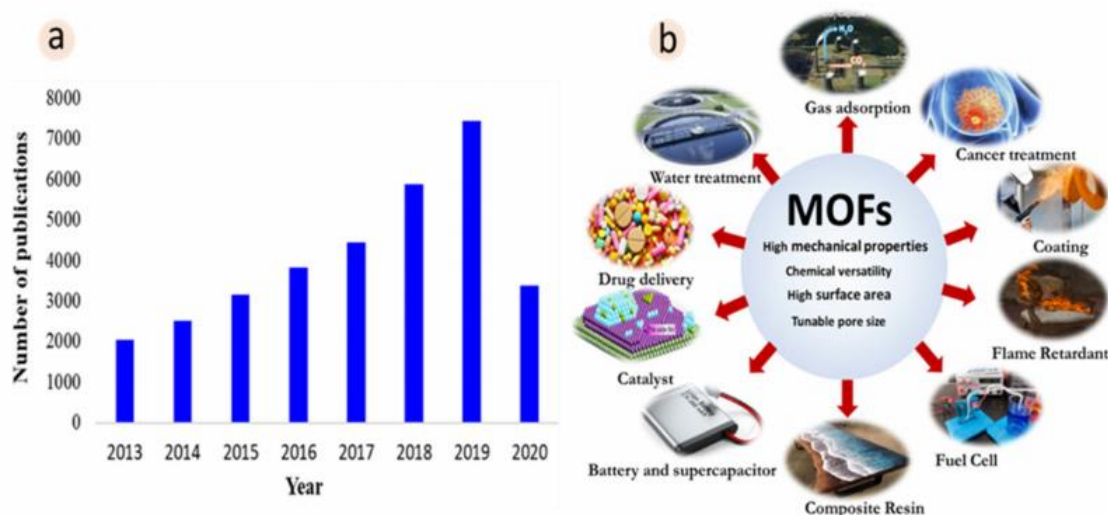

Fig.I.1-1. (a) number of publications related to MOFs in the period of 2013 to 2020, (b) various applications of MOFs
Source: Mashhadzadeh, A.H., Taghizadeh, A., Taghizadeh, M., Munir, M.T., Habibzadeh, S., Salmankhani, A., Stadler, F.J., Saeb, M.R., J. Compos. Sci., 4(2) (2020), 75:88.

The general strategy of synthesis for MOFs is to use a divergent ligand that has at least two donor atoms which can form a linking bridge between metal ions or clusters, as it can be observed in Figure I.1-2. Building blocks are brought together in liquid phase, using the solvent as a medium to induce the self-assembly process that generates the framework, the reaction usually taking place at room temperature or under hydro/solvothermal conditions [10,12]. There are several factors which influences the synthesis, part of which derive from the assembly units and are detailed in the following subchapter.
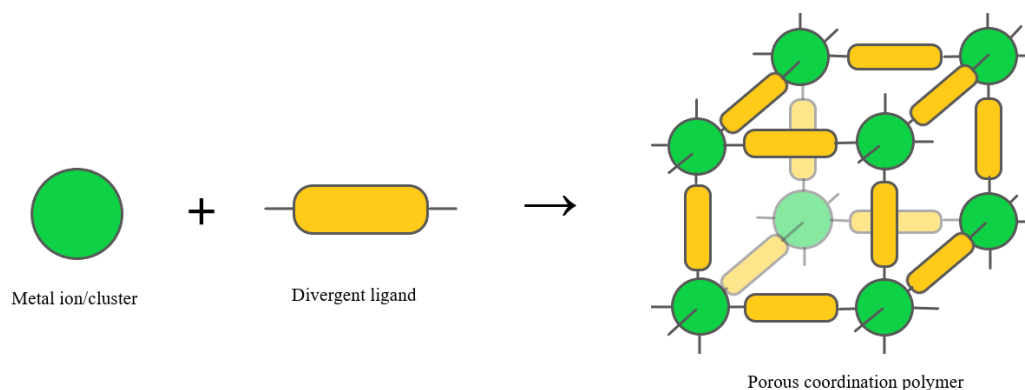

Fig.I.1-2. Schematic representation of the strategy for synthesis of PCPs

I.2. Structural features and physical properties of PCPs

I.2.1. Building blocks for PCPs

The building blocks of coordination polymers are usually classified in *connectors* (metal ions or clusters) and *linkers* or *spacers* (bridging ligands) [13]. Connectors have different shapes and sizes, depending on the stereochemistry of the metal ion (e.g., linear, angular, T-shape, trigonal-planar, tetrahedral), its size, chemical hardness/softness [14], influencing the dimensionality and structural motifs of the obtained coordination polymer. The tetrahedral and octahedral geometries are widely used because of their tendency to form 3D architectures, but also because they can generate other different geometries through the use of blocking ligands.

Linking groups have to be multidentate exo-type ligands in order to obtain the extended network of the coordination polymer. Important features of linkers include charge, the most common being the neutral (Figure I.2.1-1.) and anionic (Figure I.2.1-2.) ligands, as well as the shapes, lengths and sizes of the core, the overall rigidity of the ligand, and orientation of the donor groups [13,14].

Besides the building blocks, auxiliary components such as counter ions, nonbonding guests or template molecules are present in the structure of the final compound [12]. The void

space within the structure is occupied by guest molecules, usually solvent molecules and/or counter ions, provided by the metal salt which will also satisfy the charge balance. The formation of weak non-covalent interactions within the final packing of the solid provides further stability to the compound.
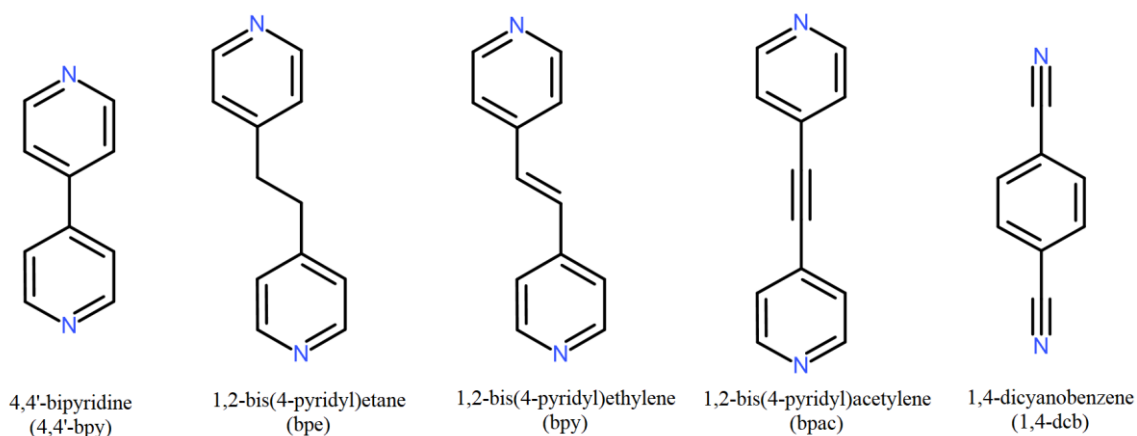
Fig.I.2.1-1. Common neutral ligands (adapted)
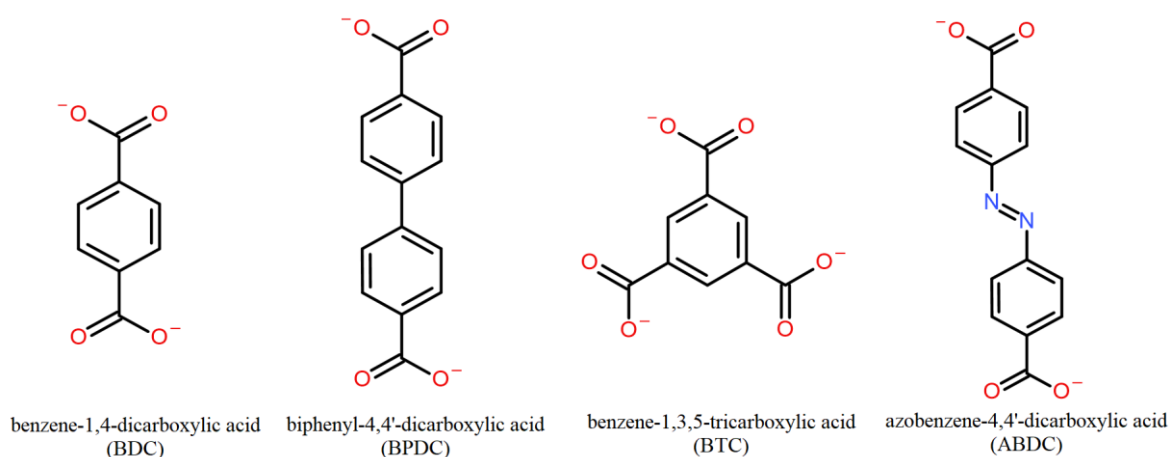*Source:* Robin, A.Y., Fromm, K.M., Coord. Chem. Rev., 250(15-16) (2006), 2127:2157

Fig.I.2.1-2. Common anionic ligands (adapted)
Source: Robin, A.Y., Fromm, K.M., Coord. Chem. Rev., 250(15-16) (2006), 2127:2157

I.2.2. Dimensionality and structural motifs

The dimensionalities of the PCPs depend on how the building blocks are organized in the structure, mainly on how the metal atoms coordinate the ligands considering that most ligands have a rod-like structure. The stereochemistry of the metal atoms has an important role in the formation of 1D or 2D coordination polymers or 3D frameworks and is a function of the coordination number characteristic to the metal [13]. In certain coordination systems, the counter anions, introduced additionally to the system or provided by the metal salt, have a

higher influence on the arrangement of the building blocks and control the resulting architectures [15,16]. Therefore, a way to control the dimensionality, as well as the structural motifs of a coordination polymer is by using the proper metal salt.

Structural motifs describe the arrangement of metal atoms and organic ligands within the structure of the coordination polymers, based on the stereochemistry of the metal and the number of coordinated ligands. As such, for 1D motifs, the metal atom is coordinated by two divergent ligands, leading to infinite chains, while in the 2D motifs there are three or four ligand molecules coordinated to the metal ion which expand on two directions. 3D motifs are formed using four or six ligands depending on the geometry of the metal which in most of the cases is tetrahedral or octahedral [17]. As shown in Figure I.2.2-1., the most common motifs for 1D PCPs are: linear, zigzag, double chain, helix, ladder, fish bone, and railroad; for 2D – honeycomb, brickwall, herringbone, bilayer; and for 3D – diamondoid, octahedral, and NbO net.
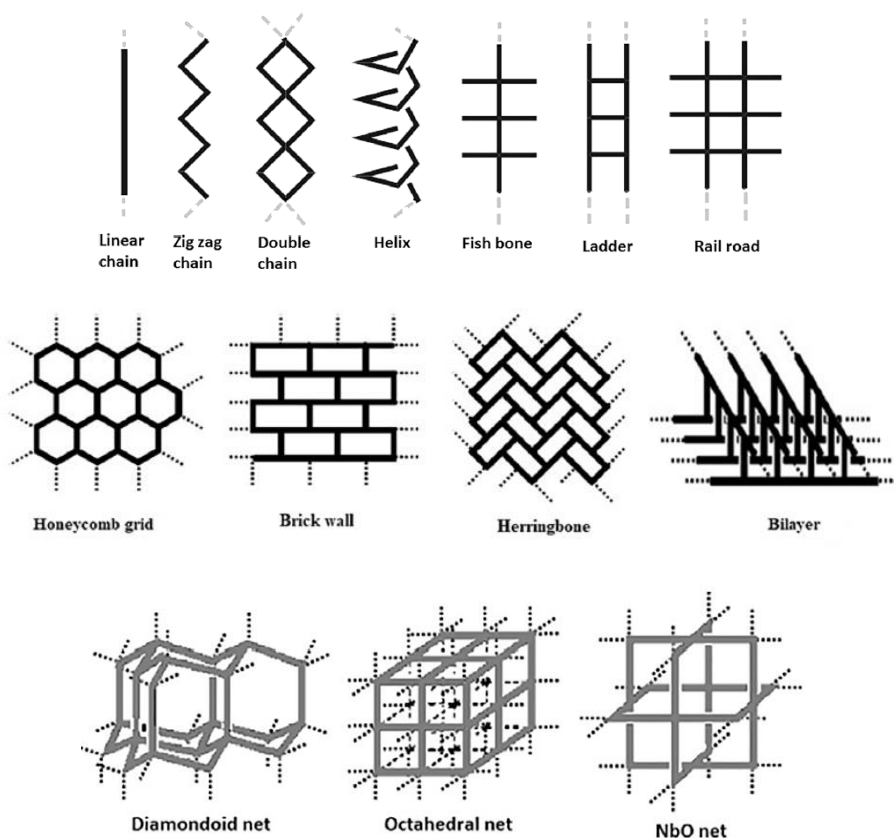

Fig.I.2.2-1. 1D (top), 2D (middle) and 3D (bottom) motifs of coordination polymers
Source: Ghosh, A., Hazra, A., Mondal, A., Banerjee, P., Inorg. Chim. Acta, 488 (2019), 86:119

I.2.3. Porosity and Flexibility

Porosity is essential in designing high performance materials mainly for storage, due to the empty space that is formed, but also for catalysis, because it provides a high surface area which is important for the catalytic process. Another application determined by porosity is separation; coordination polymers can be used in separation processes in the same fashion as zeolites. Due to its importance for previously mentioned applications, many studies have focused on increasing the porosity limit while maintaining the robustness of the polymer [18].

The easiest control of the pore size can be obtained by varying the length of ligands within the same type of network [9]. For large pore sizes however, it may be possible for the structure to collapse in the absence of a guest molecule or at its removal. At the same time, the catenation effect may occur, in which interpenetrating structures are formed in order to minimize the free space in the packing of the constituent particles in solids. A selection of pore structure in a series of different MOFs is illustrated in Figure I.2.3-1.
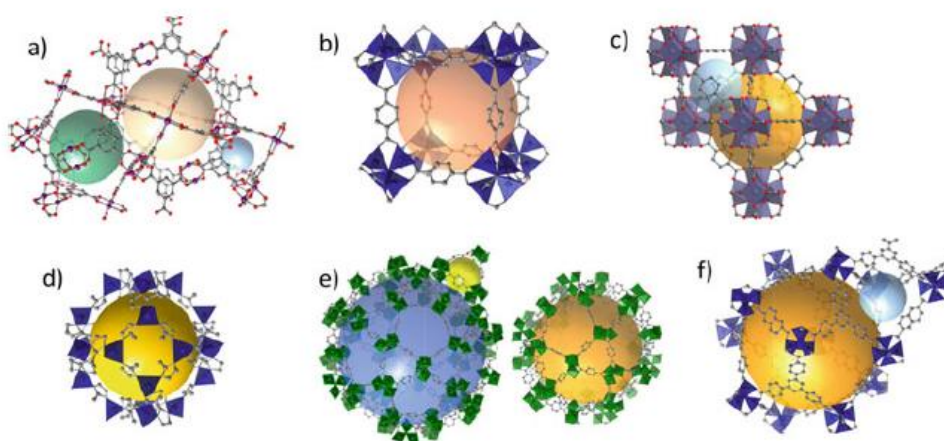

Fig.I.2.3-1. Pore structures in HKUST-1 (a), MOF-5 (b), UiO-66 (c),
ZIF-8 (d), MIL-101 (e), DUT-6 (f)
Source: Bon, V., Senkovska, I., Kaskel, S., Chapter 6: Metal-Organic Frameworks in Nanoporous Materials for Gas Storage, Green Energy and Technology, (2019), 137:172.

Flexibility is the property of porous coordination polymers to reversibly change their structure upon applying external stimuli, such as: guest molecules, heat, an electro-magnetic field, giving an advantage to these compounds over the other porous materials (zeolites and activated carbon). Guest molecules are the main factor that influences flexibility of PCPs, and can be classified into - rotation of bridging ligands (a), shape fitting response (b) or interpenetration (c) [19], as can be seen in Figure I.2.3-2.
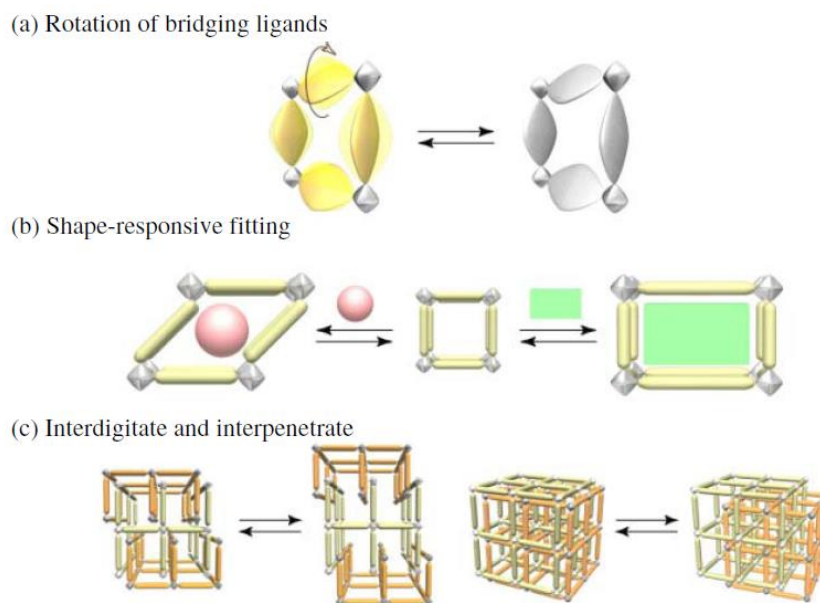
Fig.I.2.3-2. Schematic representation of PCPs flexible property
Source: Bureekaew, S., Shimomura, S., Kitagawa, S., Sci. Technol. Adv. Mater., 9(1) (2008), 014108

I.3. Applications of PCPs

Given their unique intrinsic properties, PCPs have found a wide variety of domains were they can be applied. Starting from areas that rely on their porosity, such as adsorption and separation, catalysis and even biomedical field, to applications focused on the metal ions properties like magnetism and luminescence. The usage of PCPs in the fields of catalysis and gas storage is presented below.

I.3.1. Catalysis

PCPs are used in catalysis due to their unique features and, although these compounds do not expose many coordinatively unsaturated metal sites, which could act as active catalytic sites, alternatives are used to prepare PCP-based type catalysts. Amongst these, the most accessible are: the use of functional organic sites [20], incorporation of nanocatalysts [21], or the structural modification in order to add unsaturated coordinative metal sites [22]. Also, post-synthetic modifications may be used in order to tune coordination polymers for catalysis or to create PCP-based catalysts.

Functional organic sites

Hasegawa *et al.* underlined the importance of functional organic sites in catalytic processes by using a tridentate ligand containing amide groups to develop a Cd(II) PCP-

based catalyst for Knoevenagel condensation reactions [20]. The synthesized compound, $\{[Cd(4-btapa)_2(NO_3)_2]\cdot 6H_2O\cdot 2DMF\}_n$, where 4-btapa = 1,3,5-benzene tricarboxylic acid tris[N-(4-pyridyl)amide] , consists of octahedral Cd^{2+} ions coordinated by six different ligand molecules. The arrangement of connectors and linkers generates six-membered ring composed of three octahedral Cd(II) and three 4-btapa units which interpenetrates to form 3D channels in the crystalline structure. The extended structure of $\{[Cd(4-btapa)_2(NO_3)_2]\cdot 6H_2O\cdot 2DMF\}_n$ is presented in Figure I.3.1-1.
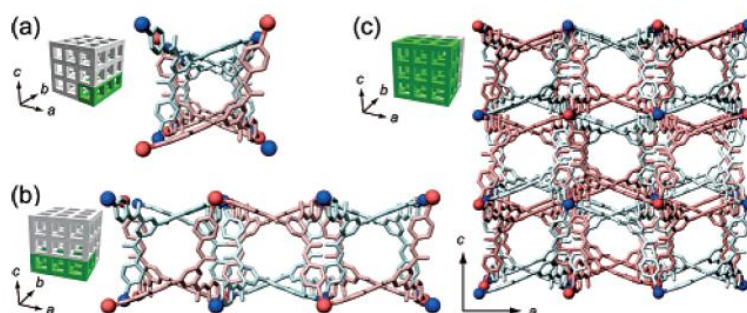
Fig.I.3.1-1. 3D crystal structure of $\{[Cd(4-btapa)_2(NO_3)_2]\cdot 6H_2O\cdot 2DMF\}_n$
Source: Hasegawa, S., Horike, S., Matsuda, R., Furukawa, S., Mochizuki, K., Kinoshita, Y., Kitagawa, S., J. Am. Chem. Soc., 129(9) (2007), 2607:2614

The amide functional group has two types of hydrogen-bonding sites: the electron acceptor –NH and the electron donor –C=O parts which are working as interaction sites with the substrate during the catalytic process. The Knoevenagel condensation reaction was performed using the benzaldehyde and three methylene compounds (malononitrile, ethyl cyanoacetate and cyano-acetic acid *tert*-butyl ester) with the Cd(II) PCP-based catalyst. The result revealed that the reaction takes place within the channels and not on the surface of the catalyst. High conversion values are obtained for substrates close to the dimensions of the channels, 4.7 x 7.3 Å, as the substrate molecules have to fit into the channels for the reaction to proceed [20].

Nanocatalysts

When incorporating metal nanoparticles, the coordination polymers act as support, but also as a template because the walls of PCPs framework apply constrains, restricting the growth and yielding to a uniform size distribution of the nanoparticles. El-Shall *et al.* conducted a study in which they incorporated Pd, Cu and Pd-Cu nanoparticles, respectively,

into MIL-101, a chromium-based metal-organic framework for the catalytic oxidation of carbon monoxide [21].

MIL-101 supported nanocatalysts where obtained using two methods based on the simultaneous activation of the pores and the rapid chemical reduction of the metal precursors using hydrazine and microwave irradiation. The first method consists in addition of metal nitrate to an aqueous dispersion of MIL-101, followed by the addition of hydrazine and heating with microwave irradiation. In the second method, the MIL-101 was stirred in the nitrate solution, separated by centrifugation, and then it was redispersed in water following the addition of hydrazine and heating with microwave irradiation [22]. Higher loadings of nanoparticles were obtained using the first method.

Unsaturated coordinative sites

To use unsaturated coordinative metal sites, supplementary anchor points are required in the structure of the ligand that can coordinate to metal ions. The desired active metal site must not be involved in the formation of the framework and should have space available for interaction with the substrate molecules. In this regard, bridging ligands with acidic or basic functional groups, such as carboxylic or sulfonic and amine group, respectively, are a good choice in the synthesis of such compounds [22]. Chen *et al.* obtained a chromium-based porous coordination polymer having unsaturated chromium ions by using an isophthalic acid ligand modified with sulfonic groups. The compound was used as an acid catalyst to transform glucose into 5-hydroxymethylfurfural (HMF) in a biomass recovery process due to the fact that is representing a renewable and sustainable alternative to fossil resources. The catalyst was prepared using a hydrothermal method by self-assembly of monosodium 5-sulfoisophthalate with metal ions and high conversion values were reported [23].

I.3.2. Gas storage

Due to their adsorption properties, porous coordination polymers were rapidly recognized as gas storage and separation materials. Kitagawa *et al.* were the first to report the methane adsorption in 1997-2000, using three-dimensional frameworks build from 4,4'-bipyridine linkers and M(II) = Co, Ni, Zn connectors. In 2003, the first hydrogen storage measurements performed on isoreticular MOF-5 and IRMOF-8 were reported by Yaghi *et al* [9,24].

PCPs exhibit high gravimetric and volumetric storage capacity and also a stronger interaction with the gas molecules [24], which gives an advantage to these compounds over

other porous materials. However, the most important feature for a higher uptake of gas molecules is the pores size, influencing the gas storage at both high and low pressures [9]. When the pore dimension is closer to the size of the gas molecules a stronger interaction will be formed which will lead to a better adsorption of the guest into the pores.

On the background of heavy industrialization and chemicals production, which in turn have negative effects on both the environment and society (i.e. high atmospheric pollution, consumption of resources and the increase of the ever-present greenhouse effect) a better control or even a decrease of these effects is mandatory. This can be achieved with the use of metal organic frameworks to alleviate the greenhouse effect caused by the carbon dioxide, to control the toxic gases, such as carbon monoxide, ammonia, and hydrogen sulfide and to widespread the clean energy through the use of energy-related gases (hydrogen and low molecular weight hydrocarbons) [25].

Carbon dioxide storage

Large amounts of carbon dioxide are released during the combustion of fossil fuels for the energy production. PCPs separate and capture the carbon dioxide from the gas mixture based on the different interaction of gas molecules with the frameworks.

CO_2 capture using PCPs are performed in the following situation: post-combustion capture, pre-combustion capture, oxy-fuel combustion, and direct capture from air. In the post-combustion capture, carbon dioxide is absorbed at low pressure, usually atmospheric pressure, while in the pre-combustion, captured of fuels must first undergo decarbonation and the carbon dioxide is adsorbed at high pressures (5-40 bars) in order to obtain zero CO_2 during the combustion step. Oxy-fuel combustion implies the use of nearly pure O_2 and will result in almost completely CO_2 generated gas, after the removal of water, thus facilitating the capture step [25].

De *et al.* synthesized two isostructural porous coordination polymers using a linear tetracarboxylic acid ligand, decorated with amino groups, and zinc or copper nitrates, respectively. The Cu-based MOF proved to be more stable and allows the removal of the solvent molecules leading to a high porous surface and thus, becoming a good candidate for hydrogen, methane, and carbon dioxide adsorption. The porous structure of Cu-MOF is illustrated in Figure I.3.2-1. The CO_2 adsorption and desorption isotherms at 0 and 25 °C revealed that the CO_2 adsorption capacity of Cu-MOF reaches the values of approximately 90 cm^3g^{-1} and with the decrease of temperature the adsorbed CO_2 volume increases reaching almost 200 cm^3g^{-1} at 0 °C [26].
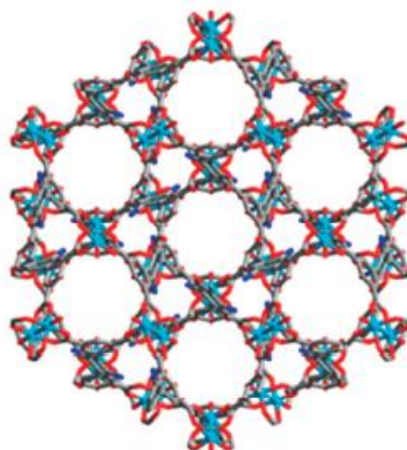
Fig.I.3.2-1. Structure of Cu-based MOF for CO₂ adsorption
Source: De, D., Pal, T.K., Neogi, S., Senthilkumar, S., Das, D., Gupta, S.S., Bharadwaj, P.K., Chem. Eur. J., 22(10) (2016), 3387:3396

Hydrogen storage

Hydrogen is an excellent alternative for coal and gasoline because of its ultrahigh gravimetric combustion heat and benign combustion products. At the same time, hydrogen could improve the environment if it would be used as fuel for automobiles. Two techniques are exploited for the hydrogen storage with the use of porous coordination polymers: cryo-temperature storage which implies the retaining of hydrogen in a tank filled with PCPs at usually 77 K, relatively low pressure (below 100 bars), and room-temperature storage. Because of the weak interactions of the PCPs with the surface at room temperature, hydrogen adsorption does not work efficiently [25]. The structure of MOF-177, a compound used for hydrogen storage, is presented in Figure I.3.2-2.
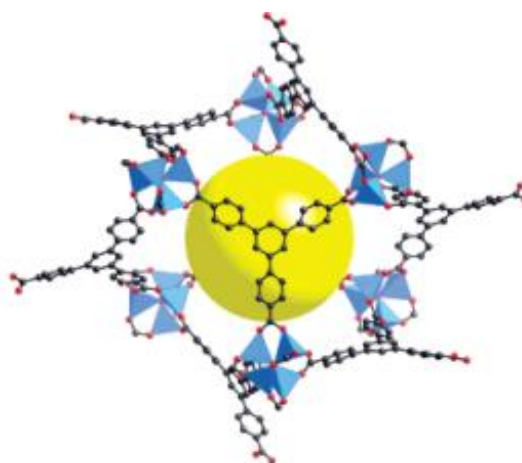

Fig.I.3.2-2. Structure of MOF-177
Source: Saha, D., Deng, S., Tsinghua Sci. Technol., 15(4) (2010), 363:376.

Hydrocarbons storage

Hydrocarbons adsorption by porous coordination polymers takes place via van de Waals interactions between the hydrocarbons and the frameworks and also uses of the flexibility of the PCPs for a better uptake depending on the hydrocarbon concentrations [25]. Besides hydrogen, methane is another fuel alternative due to its low carbon emission and thermal efficiency and also because of its abundance, being the major component of natural gas [28]. Due to its potential, many studies focused on the methane adsorption using different PCP architectures.

Acetylene is the simplest alkyne and is widely used as gas for oxy-acetylene welding and metal cutting and is a key starting material for electronic materials, as well as in manufacturing of various fine chemicals, such as vinyl chloride and methyl acrylate [28].

Jiang *et al.*reported the synthesis of MOF materials based on the Zn_4O cluster, benzene-1,3,5-tri-β-acrylic acid (H$_3$BTAC) ligand and a series of functionalized benzene dicarboxylic acids (H$_2$DBC) linkers. The structure of MOF-905, one of the compounds used can be observed in Figure I.3.2-3. These compounds were used for methane adsorption at both low and high pressure and room temperature. The results shown methane uptake between 7.7-11.0 cm^3g^{-1} at low pressure (1.1 bar) and an increase of the loading capacity of approximately 39 times at high pressure (80 bar), the highest value obtained being 310 cm^3g^{-1} [29].
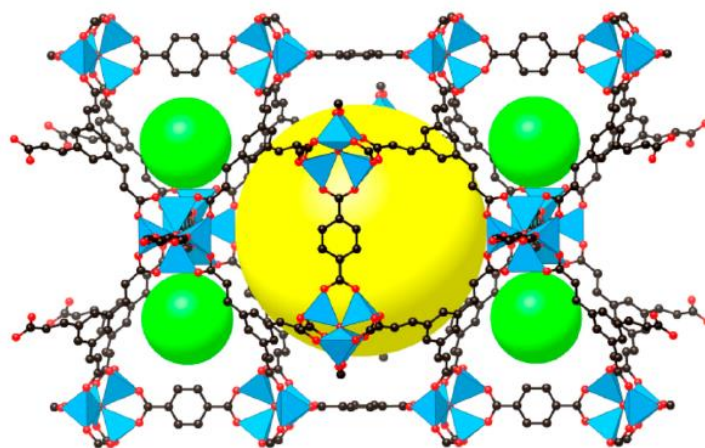

Fig.I.3.2-3. Structure of MOF-905 with the octahedral (yellow) and tetrahedral (green) cages
Source: Jiang, J., Furukawa, H., Zhang, Y.-B., Yaghi, O.M., J. Am. Chem. Soc., 138(32) (2016), 10244:10251

Yuan *et al.* obtained a porous coordination polymer based on copper clusters and isophthalate ligands that show high acetylene uptake at ambient conditions. An interesting feature of this compound is the pore distribution which defines three types of nanocages with

pore diameters of 15, 12 and 8 Å, respectively. The acetylene adsorption test revealed a very good uptake at room temperature, around 220 cm^3g^{-1} and maximum uptake of 280 cm^3g^{-1} achieved at 0 °C [28].

Toxic gases storage

The separation and storage of toxic gases, such as carbon monoxide (CO), nitrogen oxides (NO, NO_2), ammonia (NH_3), sulfur dioxide (SO_2), and hydrogen sulfide (H_2S) are related to human health and chemical production [25].

Leroux *et al.* obtained a Cd-based porous coordination polymer with piridinium carboxilate ligands (Figure I.3.2-4.). The compound has tetrameric building blocks that generate hexagonal channels in the final structure of the compounds. The adsorption tests had shown a high ammonia uptake at room temperature, reaching a maximum of 22.8 mmol/g at 900 hPa that corresponds to 0.39 g of ammonia per 1 g of compound [30].
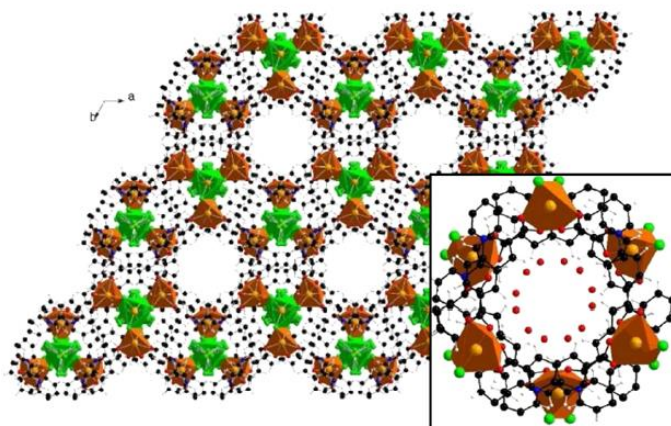

Fig.I.3.2-4. General view of Cd-based PCP showing hexagonal channels
Source: Leroux, M., Mercier, N., Allain, M., Dul, M.-C., Dittmer, J., Kassiba, A.H., Bezverkhyy, I., Inorg. Chem., 55(17) (2016), 8587:8594

Belmabkhout *et al.* developed a series of isostructural metal-organic framework with square-octahedral topology (soc-MOF), using azobenzene tetracarboxylic acid (ABTC) linking groups and different oxo-centered trinuclear metal cluster (M = In^{3+}, Fe^{3+}, Ga^{3+}, Al^{3+}). The general structure of the $\{[M_3O(ABTC)_6]\}_n$ compounds can be seen in Figure I.3.2-5. The gas adsorption was performed for carbon dioxide, different hydrocarbons with low molecular weight and hydrogen sulfide. The results revealed that H_2S exhibits high affinity towards the Ga-based compound, which can be explained by the favorable binding to the exposed and coordinatively unsaturated M^{3+} open metal sites [31].
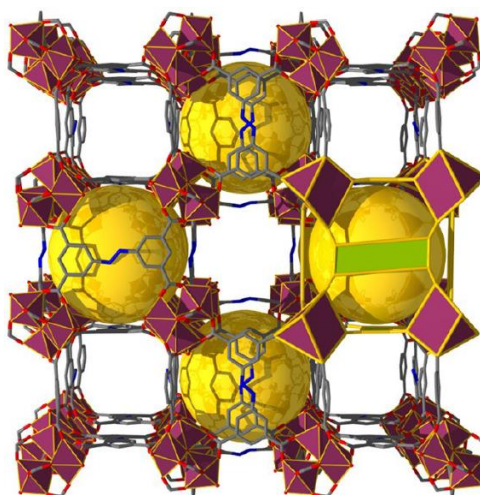
Fig.I.3.2-5. Structure of $\{[M_3O(ABTC)_6]\}_n$ compounds
Source: Belmabkhout, Y., Pillai, R.S., Alezi, D., Shekhah, O., Bhatt, P.M., Chen, Z., Eddaoudi, M., J. Mater. Chem. A, 5(7) (2017), 3293:3303

I.3.3. Ion exchange/sorption

This application relies on the MOFs property to interact with external chemicals, notably ionic species, and is usually implemented in water treatment, as most pollutants are heavy metals ions (Hg^{2+}, Pb^{2+}, Cd^{2+}) or anionic species (CrO_4^{2-}, CN^-, NO_3^-, ClO_4^- etc).

Conventional material, such as organic resins and inorganic materials (zeolites and layered double hydroxides – LDHs), have been investigated for their ion-exchange properties but each of them suffers from different drawbacks: in the case of organic resins - poor regeneration, relatively low thermal and chemical stability and for LDHs or zeolites - slow sorption kinetics and limited selectivity. In this regard, MOFs that exhibit ion-exchange/sorption properties may be considered as a next-generation of materials because it combines a highly-ordered porous structure, which is not typical for organic resins, and a large variety of binding groups that are not present in traditional inorganic ion exchangers [32].

Ion-exchanging MOFs are designed to work mostly as anion-exchangers and their synthesis employs the use of neutral polytopic organic ligands like DABCO (1,4-diazabicyclo[2,2,2]octane) and poly-pyridines [32], by combining these neutral ligands with polycarboxylate compounds [33] or through the use of ligands that possess both neutral and anionic points for coordination to metal ions. Other methods employ the post-synthetic ligand or metal ion exchanges [34] which can be used for tuning neutral MOFs for ion-exchange or enhancing MOFs that have an ionic framework.

Chapter II. Experimental Part

II.1. Synthesis of Cu-based PCPs with Kagomé layers

Three-dimensional Cu-based porous coordination polymers were obtained using $Cu(BF_4)_2 \cdot 6H_2O$ or $Cu(ClO_4)_2 \cdot 6H_2O$ salts and different exo-bidentate bipyridine-based ligands, such as: 1,2-bis(4-pyridyl)ethylene (bpy), 1,2-bis(4-pyridyl)ethane (bpe), and 4,4'-azopyridine (azopy).

In the first part of the synthesis, 1 mmol of bipyridine-based ligand was dissolved in a mixture of methanol and water, then it was added over a methanolic solution containing 1 mmol of Cu(II) salt. The resulting mixture was magnetically stirred for 30 minutes at room temperature, forming a blue/purple suspension or orange in the case of azopyridine, due to the intense color of the ligand.

During the second step, several drops of aqueous ammonia (25%) is added dropwise to the mixture yielding a clear dark blue solution (brown, when azopyridine is used) which is then stirred for another 10 minutes at room temperature. The synthesis of Cu-based porous coordination polymers is depicted in Figure II.1-1.

The final solution undergoes a slow evaporation process during which atmospheric carbon dioxide is directly fixed into the structure as carbonate (CO_3^{2-}) due to the basic conditions provided by ammonia. After several days, small blue-purple crystals are formed except in the case of azopyridine where brown crystals are formed after 2-3 weeks.
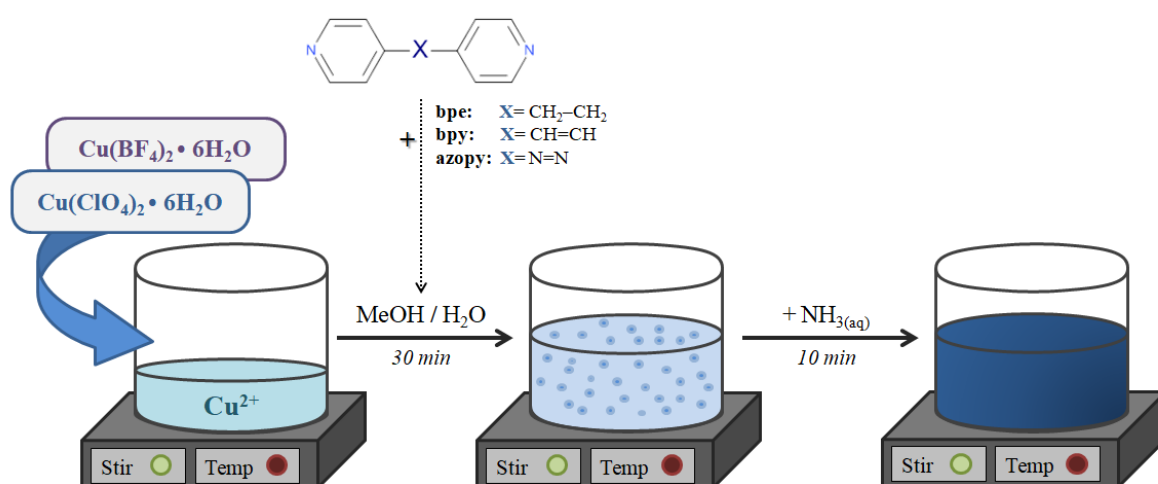

Fig.I.1-1. Synthesis of Cu-based porous coordination polymers

II.2. Characterization of Cu-based PCPs with Kagomé layers

II.2.1. Structural characterization

Single crystal X-ray diffraction revealed that all compounds crystallize in a hexagonal system, belonging to P-6 space group, and share the general formula $\{[Cu_3(CO_3)_2(L)_3](Y)_2\}_n$, where L = bipyridine-based ligand and Y = ClO_4^- or BF_4^- anions. In total, six isostructural compounds were obtained: L = bpy, Y = ClO_4^- (**1**), L = bpy, Y = BF_4^- (**2**), L = bpe, Y = ClO_4^- (**3**), L = bpe, Y = BF_4^- (**4**), L = azopy, Y = ClO_4^- (**5**), L = azopy, Y = BF_4^- (**6**). The crystallographic data of compounds **1, 2, 3,** and **6** are given in Table II.2.1-1.

Table II.2.1-1. Crystallographic parameters for **1, 2, 3** and **6**

Compound	(1)	(2)	(3)	(6)
Formula	$C_{38}H_{30}Cl_2Cu_3N_6O_{14}$	$C_{38}H_{30}B_2Cu_3F_8N_6O_6$	$C_{38}H_{36}Cl_2Cu_3N_6O_{14}$	$C_{32}H_{24}B_2Cu_3F_8N_{12}O_6$
Formula mass / gmol^{-1}	1056.20	1030.92	1062.25	1036.87
Crystal system	Hexagonal	Hexagonal	Hexagonal	Hexagonal
Space group	P-6	P-6	P-6	P-6
a/Å	9.297(5)	9.275(3)	9.396(1)	9.279(6)
c/Å	13.364(8)	13.371(4)	13.296(2)	12.961(7)
V/Å^3	1000.4(1)	996.2(7)	1016.6(3)	966.6(1)
ρ/gcm^{-3}	1.753	1.718	1.735	1.781
T/K	293(2)	293(2)	293(2)	293(2)
Z	1	1	1	1
Goodness of fit (S)	1.105	1.105	1.106	1.604
R	0.0413	0.0422	0.0876	0.1064
wR	0.1068	0.1108	0.2323	0.3264

The Cu-based porous coordination polymers consists of 2D $[Cu_3(CO_3)_2]^{2+}$ layers in the crystallographic *ab*-plane, which act as secondary building units (SBU) that are further linked one to another by the bipyridine-based ligands along the *c*-axis, yielding to a 3D pillared-layer framework of Cu atoms with mixed anionic and neutral ligands, as it can be observed in Figure II.2.1-1. Disordered ClO_4^- or BF_4^- anions are positioned along the *c*-axis and neutralize the remaining charge of the framework.
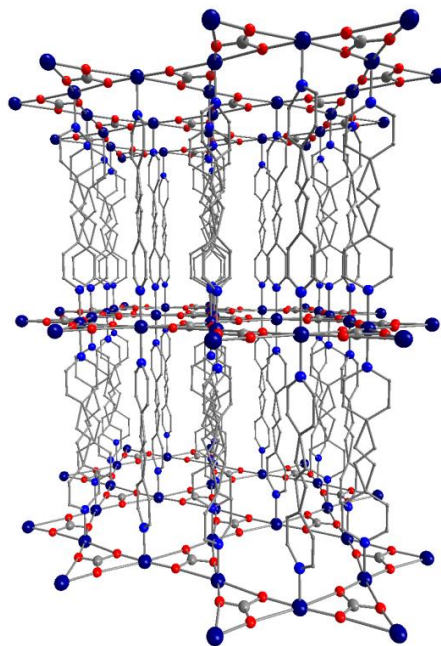
Fig.II.2.1-1. Structure of $\{[Cu_3(CO_3)_2(L)_3](Y)_2\}_n$
H atoms and counter ions were omitted for clarity.

Each Cu(II) center has a coordination number of six, displaying an octahedral geometry with disordered vertices as a result of the Jahn–Teller effect. The coordination environment of Cu(II) atoms (illustrated in Figure II.2.1-2.) is satisfied by four oxygen atoms from two crystallographically independent CO_3^{2-} anions, of which two occupy the apex positions of the octahedron and the other two form the basis of the octahedron together with two nitrogen atoms from two different bipyridine-based ligands. The specific bond lengths between the metal ion and donor atoms are in the range of 1.959(7) – 2.739(8) Å, while the specific angles vary between 51.5(1) – 131.8(2) degrees. These values differ in each compound and are detailed in Table II.2.1-2 and Table II.2.1-3.

CO_3^{2-} anions act as tridentate tris-chelated ligands and connect three different Cu(II) atoms through μ_2-oxo bridges in a planar trigonal arrangement. These trigonal units build up a perfectly planar $Cu(CO_3)$ layer with hexagonal arrangement in the crystallographic *ab*-plane, known in the literature as Kagomé layer, and is presented in Figure II.2.1-2. The Jahn–Teller axes of the Cu(II) centers lie in the plane of the Kagomé layer, leading to a concerted rotation of each carbonate unit from its regular orientation [6]. The angles have a slightly variation in the synthesized compounds, being in the 171.0(1) – 175.3(3) degrees range for Cu–O(1)–Cu angles and 172.2(3) – 179.1(2) for Cu–O(2)–Cu angles, respectively. The ClO_4^- or BF_4^- anions are in symmetry-related disorder and occupy the hexagonal pores of the Kagomé planes, as well as the void spaces between the bipyridine-based pillars.
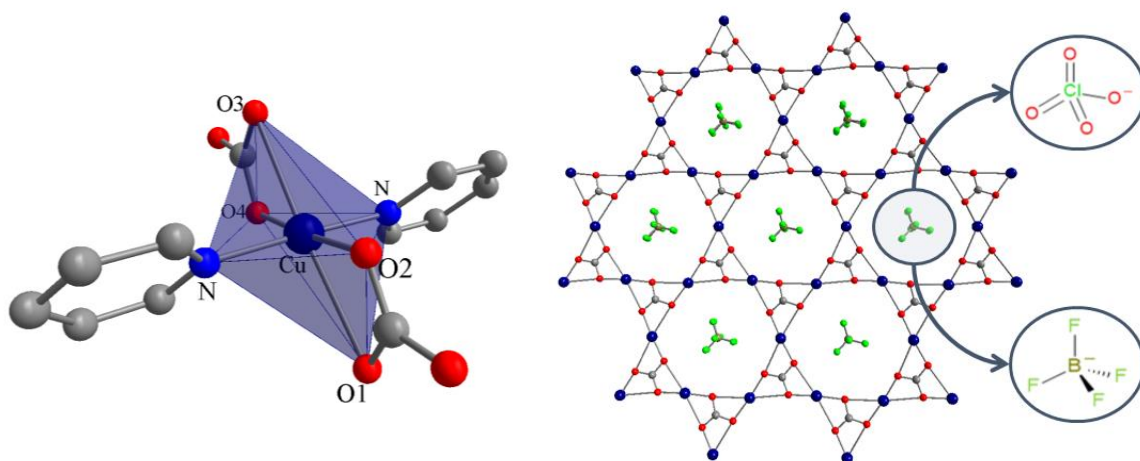
Fig.II.2.1-2. Coordination environment of Cu(II) and Kagomé layer in $\{[Cu_3(CO_3)_2(L)_3](Y)_2\}_n$ with counter anions in the hexagonal pores

Table II.2.1-2. Specific bond lengths in compounds **1**, **2**, **3** and **6**

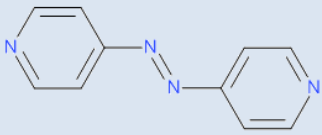| Bond	Length (Å)			
	1	**2**	**3**	**6**
Cu – O(1)	2.739(8)	2.721(6)	2.720(1)	1.995(3)
Cu – O(2)	1.959(7)	1.959(7)	1.974(1)	2.599(4)
Cu – O(3)	2.655(8)	2.650(5)	2.643(1)	2.505(2)
Cu – O(4)	1.970(6)	1.968(7)	2.080(2)	2.505(3)
Cu – N	1.999(5)	1.998(5)	2.000(1)	1.965(8)
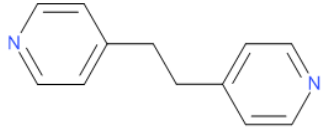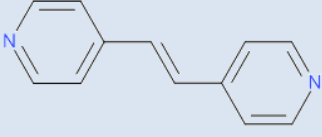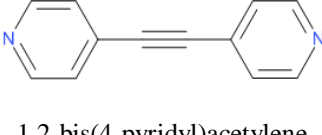
Table II.2.1-3. Specific angles in compounds **1**, **2**, **3** and **6**

Atoms	Angle (º)			
	1	**2**	**3**	**6**
O(1) – Cu – O(2)	52.3(2)	53.1(2)	55.4(5)	59.1(1)
O(2) – Cu – O(3)	120.6(2)	120.5(2)	130.5(6)	123.1(1)
O(3) – Cu – O(4)	55.3(2)	54.9(2)	51.8(8)	51.5(1)
O(1) – Cu – O(4)	131.8(2)	131.4(2)	123.1(7)	126.2(1)
O(2) – Cu – N	89.8(1)	90.0(1)	90.0(3)	92.8(6)
O(4) – Cu – N	90.2(1)	90.0(1)	90.0(3)	87.4(4)
O(1) – Cu – N	89.2(1)	89.2(1)	91.0(3)	89.7(5)
O(3) – Cu – N	90.8(1)	90.8(1)	89.0(3)	90.3(5)

The overall size of the coordination polymers is determined by the sizes of the 2D $[Cu_3(CO_3)_2]^{2+}$ layers as well as the distances between them. The size of the layer is a function of the amount of CO_2 that is fixed into the structure as this is a key factor in obtaining the Kagomé layers and may be correlated with the amount of connectors, since the SBU layers have a ratio between Cu^{2+} and CO_3^{2-} ions of 3:2.

The interlayer distance (Table II.2.1-4) provides information about the void space within the channels and is directly dependent on the length of the linkers. As expected, the distance increases from 12.960 Å to 13.603 Å with the increase of the spacer length between the two pyridyl rings. The highest value is obtained in the case of 1,2-bis(4-pyridyl)acetylene due to the linear arrangement of this molecule [6]. For 1,2-bis(4-pyridyl)ethylene and 1,2-bis(4-pyridyl)ethane ligands, the variation is given by the flexibility/rigidity of the spacer with the latter providing a shorter interlayer distance due to compression movements.

Table II.2.1-4. Interlayer distances in $\{[Cu_3(CO_3)_2(L)_3](Y)_2\}_n$

Ligand	Distance (Å)
4,4'-azopyridine	12.960 (for BF$_4^-$)
1,2-bis(4-pyridyl)ethane	13.296 (for ClO$_4^-$)
1,2-bis(4-pyridyl)ethylene	13.365 (for ClO$_4^-$) 13.371 (for BF$_4^-$)
1,2-bis(4-pyridyl)acetylene	13.606 (for ClO$_4^-$) [6]

Powder X-ray diffraction (PXRD) analysis was employed for characterization of the compounds in terms of crystalline phase purity. Each sample was grounded and then exposed to Cu-Kα radiation at room temperature, in the 5 – 35 degrees range of *2θ*. The X-ray powder diffractogram of compound **2** is presented in Figure II.2.1-3. All diffraction peaks observed in the powder XRD pattern are well defined, indicating a good crystallinity of the probe. It can be observed that the experimental pattern of diffraction corresponds with the theoretical one, generated from the crystallographic information file (cif), thus showing the purity of the crystalline phase. The intense peak obtained at 22 degrees of *2θ* is due to preferential arrangement of crystallographic planes which occurs during the grounding of the sample. This diffraction pattern was obtained in all synthesized compounds thus showing the phase purity for this family of isostructural MOFs. Diffractograms of the other compounds are attached in Appendix (section A, Figures A1 – A5).
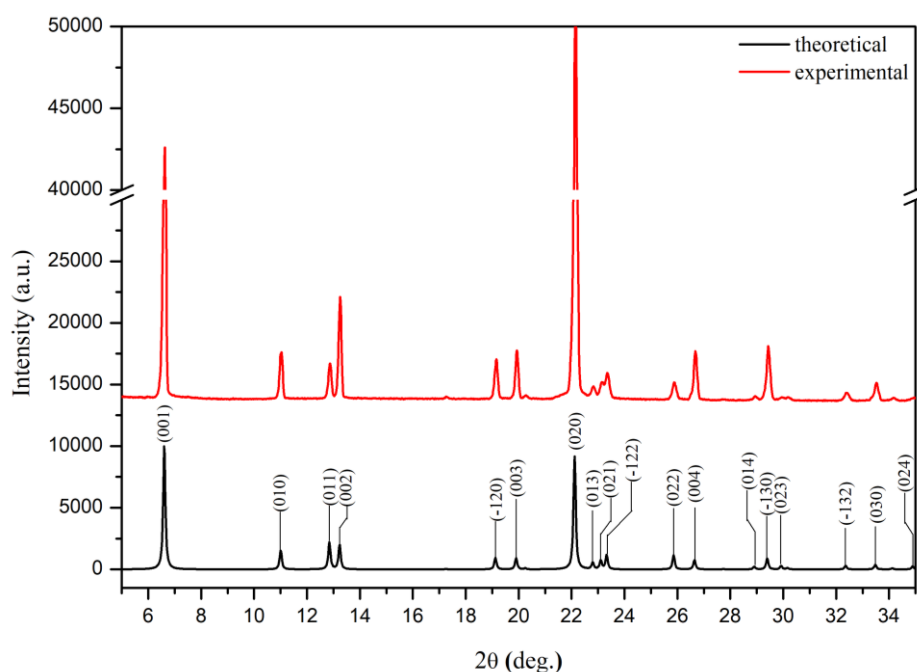

Fig.II.2.1-3. Powder XRD pattern of compound **2**

II.2.2. Spectral characterization

The infrared spectra (all IR spectra are included in the Appendix, section C, Figures C1 – C6) were recorded in the 4000 – 400 cm^{-1} range and it has been observed that all synthesized compounds follow the same pattern of peaks with very few variations, which explains the structural similarities of the compounds as well as the type of existing bonds. Around 1450, 1032 and 871 cm^{-1} one strong and two medium peaks appear and characterize

the bridging carbonate within the Kagomé layers. The bipyridine-based ligands are described by a series of peaks: two weak peaks in the $3100 - 3000$ cm^{-1}, a medium one in the $1625 - 1610$ cm^{-1} range, two weak peaks in the $1350 - 1230$ cm^{-1} range, and a weak (in the case of compounds 5 and 6) peak around 1426 cm^{-1}.

BF$_4^-$ anions are characterized by a strong peak in the $1100 - 1050$ cm^{-1} range. The infrared spectra of coordination complexes **1**, **3**, and **5** show two intense bands, at around 1100 and 630 cm^{-1} attributed to the presence of the ClO$_4^-$ anions. These bands are assigned to the anti-symmetric stretching and anti-symmetric bending vibration mode, respectively [35]. The former band is split with a poorly defined maximum showing the deformation from Td symmetry [36]. At low wavenumbers metal – donor atoms bonds may be identified, in the present compounds the stretching vibration modes of Cu–O and Cu–N bonds have a medium peak around 560 cm^{-1} and weak peaks around 440 cm^{-1}, respectively. The characteristic vibrations for each compound are given in Table II.2.2-1.

Table II.2.2-1. Characteristic vibrations (cm^{-1}) of $\{[Cu_3(CO_3)_2(L)_3](Y)_2\}_n$

Bonds	Compounds					
	1	**2**	**3**	**4**	**5**	**6**
ν C─H	3099 (w) 3051 (w)	3102 (w) 3053 (w)	3098 (w) 3050 (w) 1235 (w)	3101 (w) 3053 (w) 1236 (w)	3100 (w) 3049 (w)	3103 (w) 3051 (w)
ν C=N	1617 (m)	1617 (m)	1619 (m)	1620 (m)	1609 (m)	1609 (m)
ν CO₃	1450 (s) 1032 (m) 871 (m)	1451 (s) 1031 (m) 873 (m-s)	1443 (s) 1034 (m) 840 (m)	1444 (s) 1033 (m) 875 (m)	1450 (s) 1031 (m) 862 (m)	1450 (s) 1030 (m) 862 (m)
ν N=N	—	—	—	—	1426 (w)	1427 (w)
ν C=C	1354 (w) 1254 (w)	1355 (w) 1255 (w)	1346 (w)	1347 (w)	1330 (w)	1331 (w)
ν ClO₄⁻	1090 (s) 623 (m)	—	1087 (s) 669 (m)	—	1084 (s) 623 (m-w)	—
ν BF₄⁻	—	1056 (s)	—	1054 (s)	—	1064 (s)
ν Cu─O	556 (m)	557 (m)	546 (m)	547 (m)	557 (m)	578 (m)
ν Cu─N	437 (w)	435 (w)	447 (w)	434 (w)	445 (w)	435 (w)

The UV-Vis spectra of the Cu(II)-based compounds were recorded in solid state in the 200 – 850 nm range and are presented in Figure II.2.2-1. As it can be observed, all compounds share the same pattern of electronic transitions, with three main absorption maxima. At higher energy values (250 — 270 nm range) are the $\pi \rightarrow \pi^*$ transitions of the bipyridine-based ligands. The ligand-to-metal charge transfer (LMCT) can be assigned to the transition bands in the 360 — 385 nm range and probably involves the oxygen donor atoms of the carbonate.
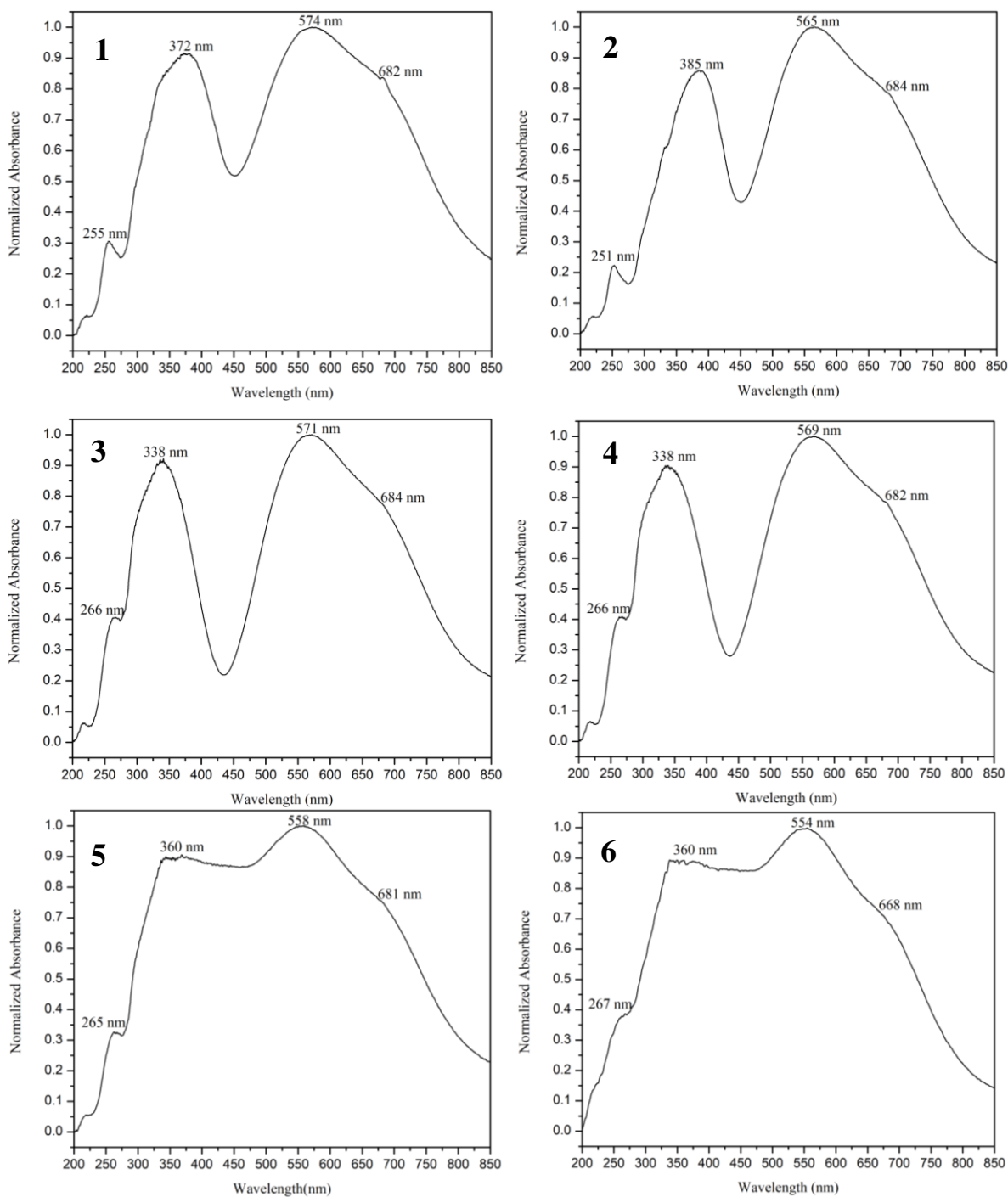
Fig. II.2.2-1. UV-Vis spectra of the obtained compounds

The wide bands in the 550 – 580 nm range can be attributed to the specific d–d transitions of Cu(II) and the shoulder around 680 nm may be explained by the Jahn─Teller distortion of the Cu(II) octahedral geometry. The large width of the bands assigned to the d–d transitions is due to the overlap of the absorption of $d_{xy} \rightarrow d_{x^2-y^2}$, $d_{z^2} \rightarrow d_{x^2-y^2}$ and $d_{xz,yz} \rightarrow d_{x^2-y^2}$ transitions which are possible for the species with square-planar or distorted octahedral stereochemistry [37].

The electronic spectra for compounds **5** and **6** are not well defined because of the presence of coloured azopy ligand which determines a brown color of the crystals and, therefore, a high absorption capacity exhibited by the compound, as can be seen in the last two (**5** and **6**) spectra in Fig.II.2.2-1.

II.2.3. Thermal stability

The thermogravimetric analysis (TGA) was performed in order to determine the thermal stability of the compounds and the results are presented in Figure II.2.3-1. It can be observed that, for compounds **1**, **3**, and **5**, the thermal decomposition is carried out in one major sharp process, similar to a total combustion, due to the presence of explosive perchlorate anions and then is followed by a broader process that continues to 600 ⁰C. The weight loss for these compounds is 86.95%, 91.46%, and 89.12%, respectively, and the residual mass corresponds to a mixture of CuO and Cu.

For the compounds with tetrafluoroborate anions (**2**, **4**, and **6**), the thermal decomposition in carried out in two subsequent steps with a total weight loss of 65.75%, 77.07% and 61.77%, respectively. As the thermogravimetric analysis was performed in an inert atmosphere (N_2) the residual mass for these compounds could be a mixture of CuO, Cu and carbon ash. The nature of the residual products will be investigated in the future.

The relatively high stability of these Cu-based MOFs is given by a series of weak interactions that spam over the whole structure, hydrogen bonds and electrostatic interactions established between counter anions and the cationic framework. The CH─π interactions are formed between the aromatic rings of the organic ligand, as presented in Figure II.2.3-2. (green dotted lines), and have distances in the 2.93 – 2.99 Å range. Although these interactions are quite weak, it provides an increased stability to the 3D framework through their number and position, spreading throughout the structure.
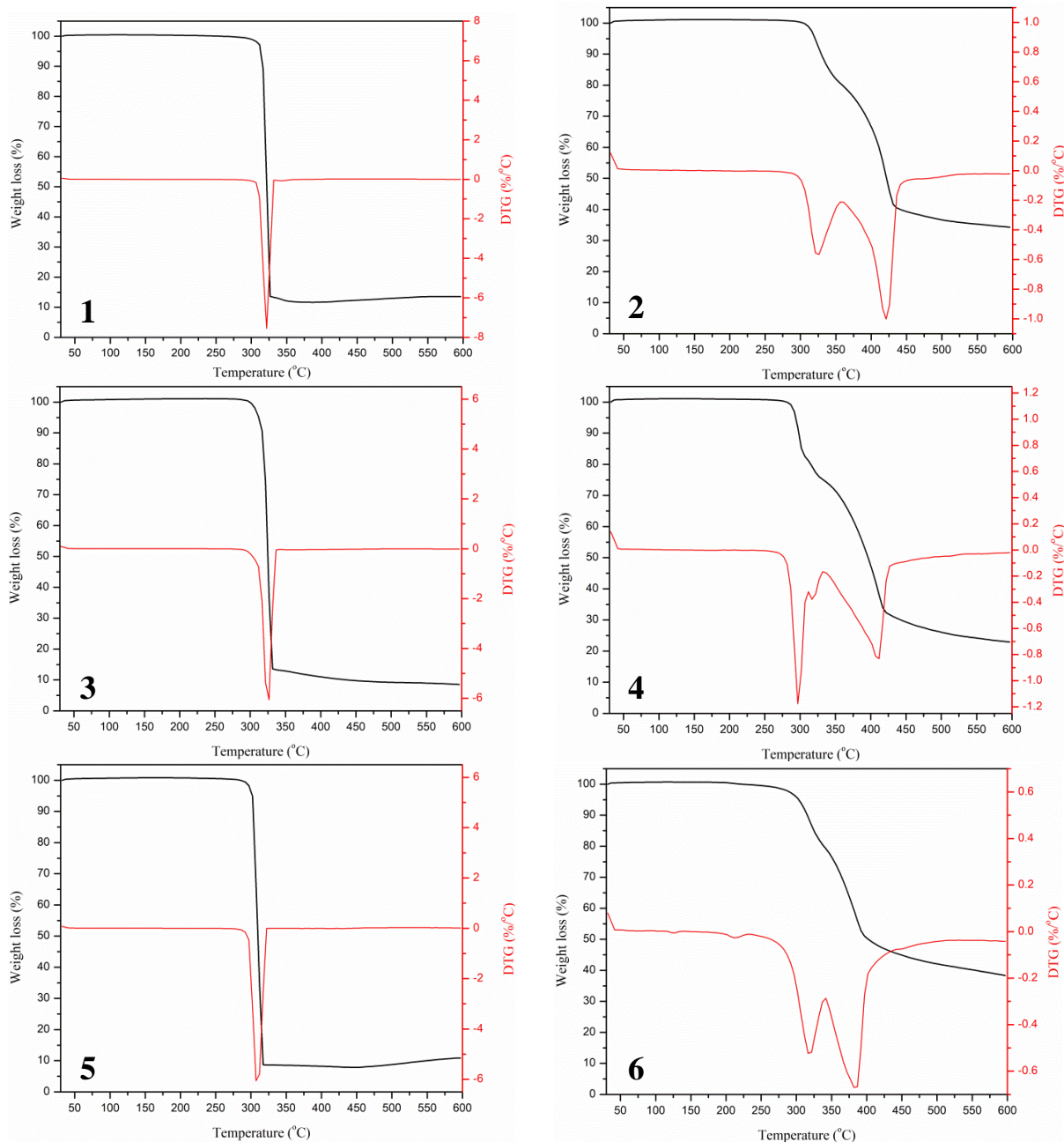
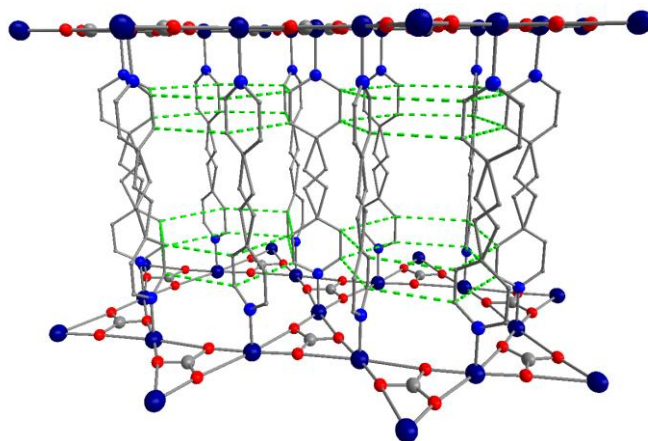**Fig.II.2.3-1.** TGA and DTG curves of the obtained compounds

Fig.II.2.3-2. CH─π interactions in $\{[Cu_3(CO_3)_2(L)_3](Y)_2\}_n$

II.3. Applications of Cu-based PCPs with Kagomé layers

II.3.1. Anion-exchange studies

MOFs that contain guest anions in the pores can undergo ion exchange. By immersion of the solids in the solution of other anion source, the guest anions of the MOFs can be exchanged with external ones. In 1990 was first reported an anion-exchange process in MOFs which happened at solid–liquid interface [38].

As revealed by crystal structure analyses, ClO_4^- and BF_4^- counter anions in the obtained MOFs are loosely bound, through weak noncovalent hydrogen bonds, to the cationic structures of the Cu-based coordination polymers. Therefore, anion exchange properties of the obtained compounds have been investigated in aqueous solutions of the appropriate salts and monitored by FT-IR and UV-Vis spectroscopies. The position of the anions along the hexagonal channel is illustrated in Figure II.3.1-1.

In this study, to investigate the anion-exchange the following categories of anions (which possess geometry and charge similarities or differences in comparison to ClO_4^- and BF_4^- ions) were employed: 1) anions with the same geometry and charge (permanganate – MnO_4^-), 2) anions with the same geometry and different charge (chromate – CrO_4^{2-}), and 3) anions with different geometry and the same charge (hexaflurophosphate – PF_6^-, nitrate – NO_3^-). At the same time, the influence of the concentration of the anion solutions on the ion-exchange process was monitored.
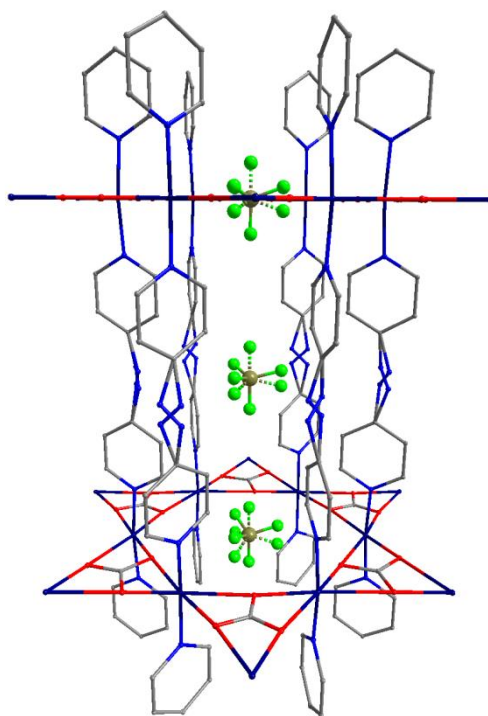

Fig.II.3.1-1. Hexagonal channels along *c*-axis in $\{[Cu_3(CO_3)_2(L)_3](Y)_2\}_n$

Low concentration of anions

Given the strong oxidizing power of MnO_4^- and CrO_4^{2-}, low concentration solutions of these anions were used in order to highlight both possible anion-exchanges and other modifications that may occur in the compounds. In this regard, 5 mg of each synthesized compound, in the solid state, were immersed in 0.1 mM aqueous solutions of MnO_4^- and CrO_4^{2-}, respectively. After three days, visual changes have been observed only in the case of the compounds containing the bpy ligand, **1** and **2**, where the pink MnO_4^- solution turned to a yellow-brown clear solution and the immersed blue-purple crystals have acquired a brownish shade. In the CrO_4^{2-} samples no changes occurred, the solution and crystals maintained the initial colours.

FTIR spectra of **1** immersed in MnO_4^- and CrO_4^{2-} solutions were recorded and are presented in Figure II.3.1-2. These two spectra are identical to the spectrum of initial **1** (Figure II.3.1-2.C). As it can be observed, there is no peak around 900 and 885 cm^{-1} that could be assigned to MnO_4^- and CrO_4^{2-} vibrations. Also, no major changes in the wavenumbers of ClO_4^- peaks (around 1100 and 620 cm^{-1}) are present, thus concluding that no anionic exchange occurs at low concentrations.
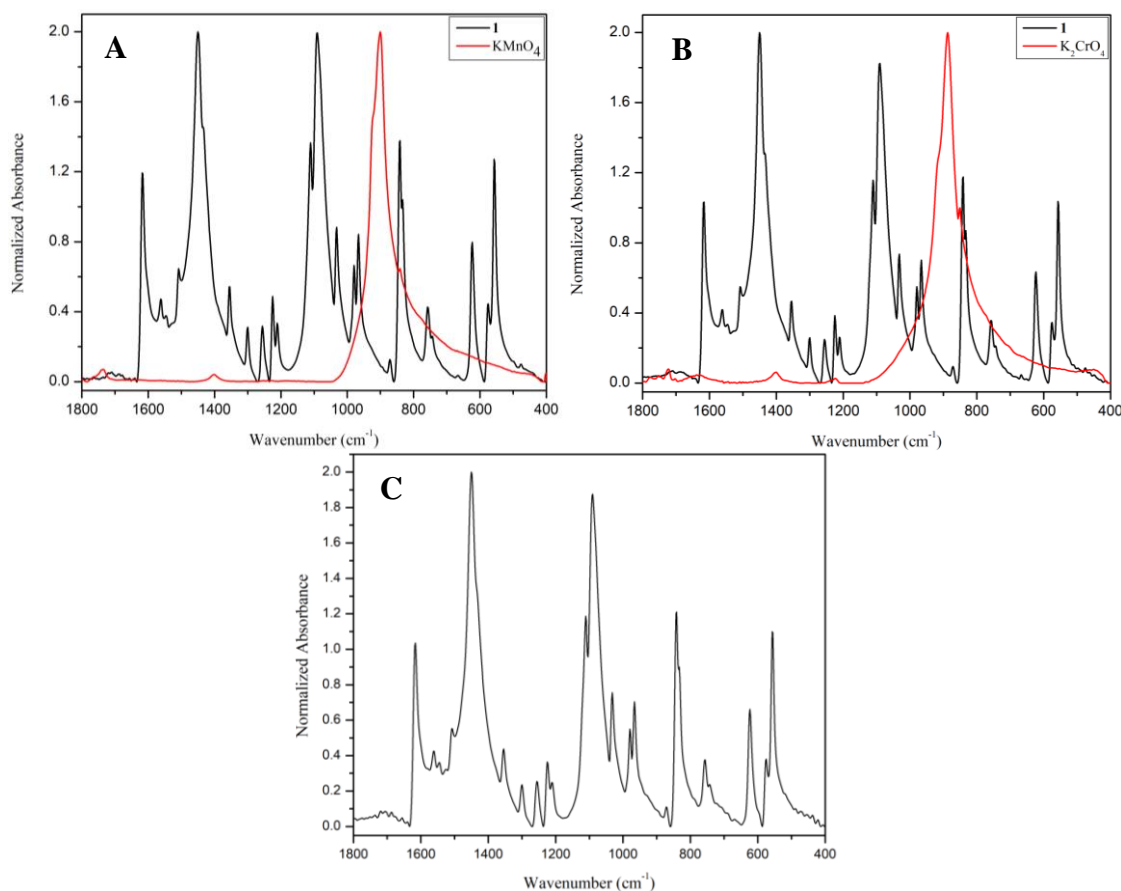

Fig.II.3.1-2. FTIR spectra of **1** immersed in 0.1 mM $KMnO_4$ (A) and 0.1 mM K_2CrO_4 (B) solutions and initial spectrum of **1** (C).

The brown colour obtained for the $KMnO_4$ samples may be explained by the presence of colloidal manganese oxide [39] formed during the oxidation of bpy ligand with $KMnO_4$. Since no oxidation conditions were provided to the system (heat or high concentration of oxidizing agent), the ligand was partially oxidized at the C-C double bond, probably forming a vicinal diol. We assume that this oxidation step is a typical mild oxidation of alkenes with Baeyer Reagent; the equation of the chemical reaction is presented in Figure II.3.1-3.

$$3\,HC{=}CH \text{ (with R1)} + 2KMnO_4 + 4H_2O \longrightarrow 3\,(\text{vicinal diol}) + 2MnO_2 + 2KOH$$
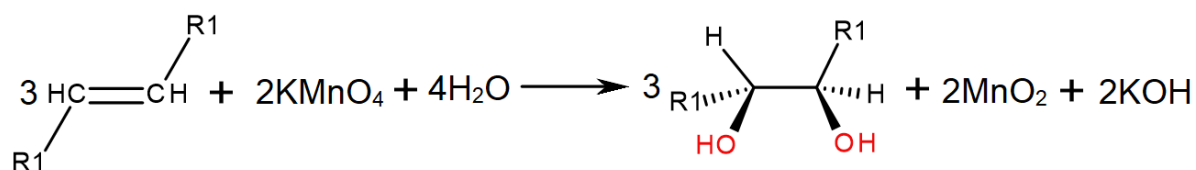
Fig.II.3.1-3. Oxidation of the ethylene derivate ligand to vicinal diol with Baeyer Reagent

The UV-Vis spectra were recorded for both solution and solid for complementary characterization. In Figure II.3.1-4 is presented the UV-Vis spectrum of the yellow-brown solution of immersed **1** and compared with the spectrum of pure $KMnO_4$ solution at the same concentration. It can be observed that the characteristic region of Mn(VII) in the 500-575 nm range is missing in the probe. At the same time, an increase of the wide band absorbance in the UV region is occurring.
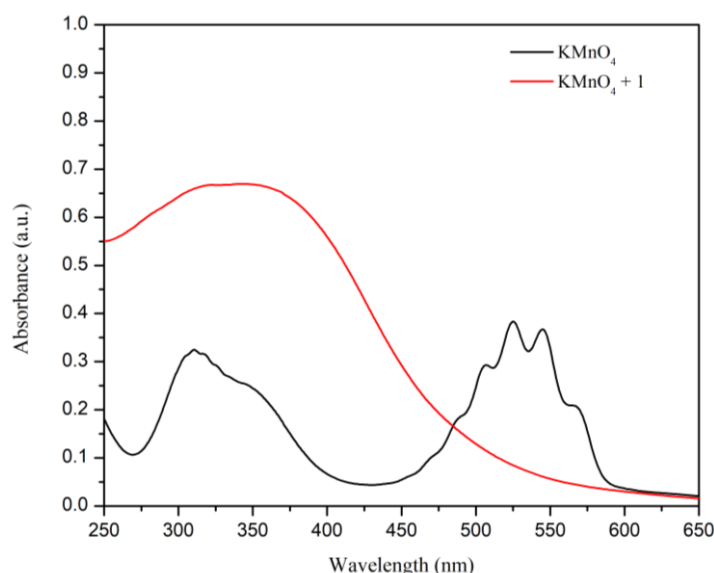

Fig.II.3.1-4. UV-Vis spectra on aqueous solutions of $KMnO_4$ (0.1 mM) and **1**+$KMnO_4$ (5 mg of **1** in 0.1 mM $KMnO_4$ solution)
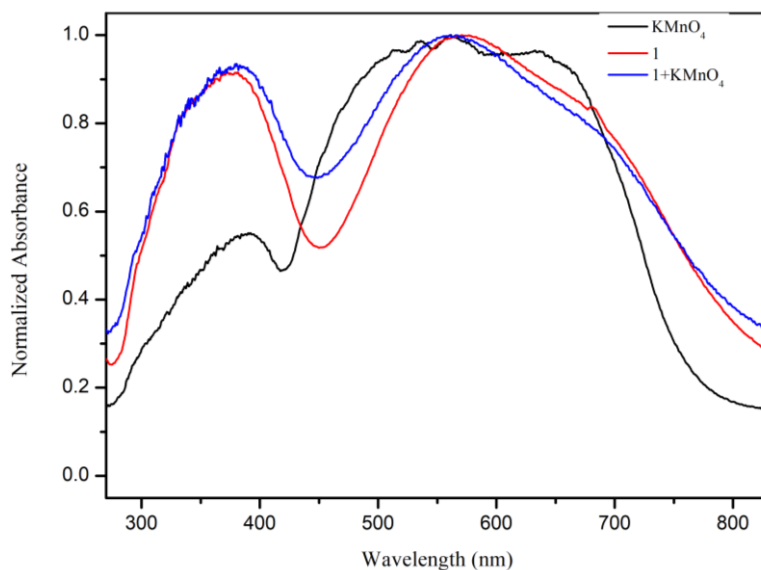
Fig.II.3.1-5. UV-Vis spectra on solid samples of $KMnO_4$ (black), **1** (red), and **1**+$KMnO_4$ (blue)

In the UV-Vis spectrum on solid samples of **1** immersed in $KMnO_4$ (Figure II.3.1-5, blue line) can be observed that the spectrum has slightly narrowed, with a bathochromic shift from 372 nm to 380 nm and a hypsochromic shift from 570 nm to 560 nm compared to the initial **1** compound (Figure II.3.1-5, red line). The $KMnO_4$ spectrum is the black line, therefore, these two shifts can be assigned to a chemical modification of **1** due to the influence of the MnO_4^- on the system.

Variation of permanganate concentration

The influence of the permanganate anion was investigated using a series of 5 solutions with concentrations in the 0.1–10 mM range, prepared according to Table II.3.1-1. To these solutions, 5 mg of **1** were added and left for 24h.

Table II.3.1-1. Concentrations and volumes used for preparation of $KMnO_4$ solutions

No.	$V_{KMnO_4}(\mu L)^*$	$V_{H_2O}\ (\mu L)$	$C_{KMnO_4}(mM)$
1	50	9950	0.1
2	250	9750	0.5
3	500	9500	1.0
4	2500	7500	5.0
5	5000	5000	10.0

* [$KMnO_4$] = 20 mM

After 24h, the initial series changed the colours from shades of pink-purple to a palette of yellow to red to purple, depending on the concentration of the solutions (Figure II.3.1-6). Significant changes can be observed from 0.1 mM to 5 mM but not in the case of the 10 mM probe because of the intense colour of the solution.

The probes were analyzed using the UV-Vis on solution and the results are presented in Figure II.3.1-7. It can be observed that the same pattern is followed, with the decrease in intensity of the band in the visible region and increase of the band in the ultraviolet region. The 5 mM and 10 mM solutions were too concentrated to measure, but a similar behaviour was noticed from diluted samples of these solutions. This means that the oxidation of the ligand occurs in the same manner as in the case of the 0.1 mM and the colour variation is given from the different ratios of colloidal Mn(IV) and Mn(VII) ions present in solutions.
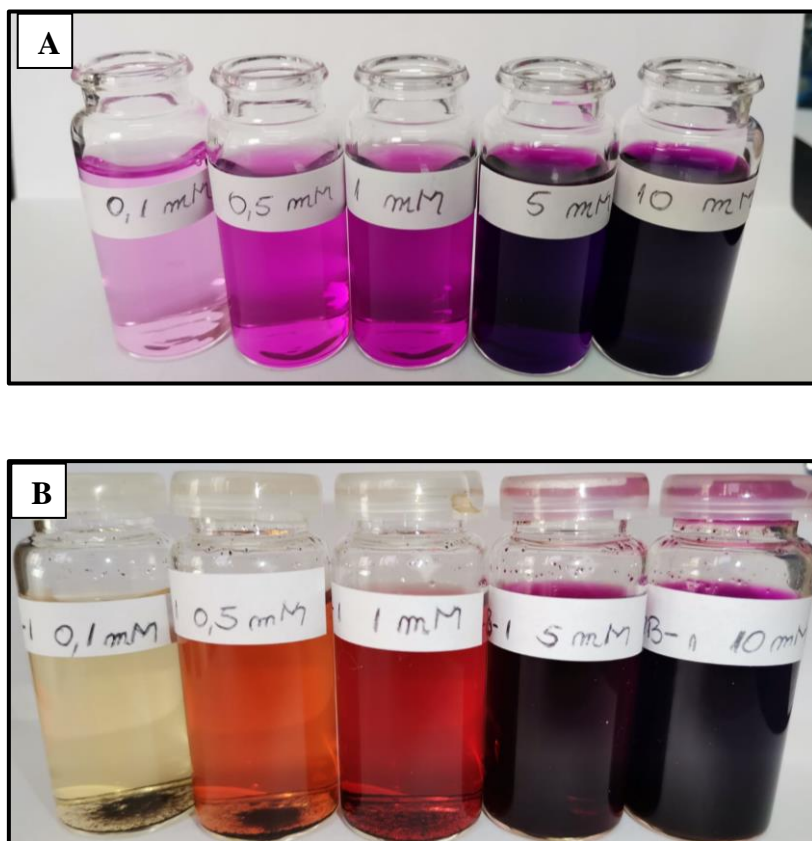
Fig.II.3.1-6. Photographs of initial series of KMnO$_4$ solutions at different concentration (A) and after 24h of contact with **1** (B)
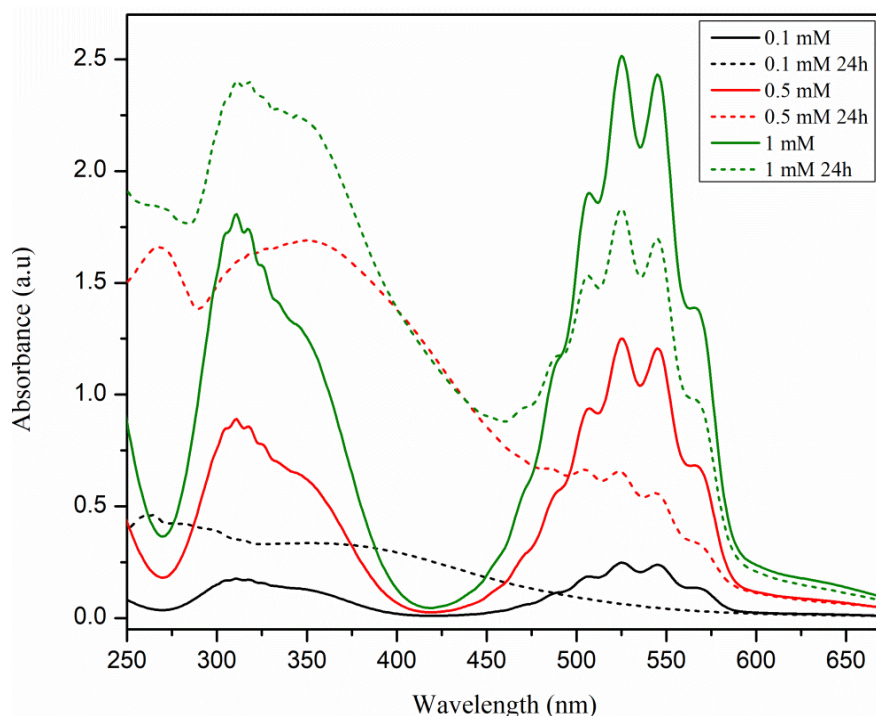
Fig.II.3.1-7. Initial series of KMnO$_4$ solutions (straight lines) and after 24h of contact with **1** (dotted lines)

High concentration of anions

To investigate the behaviour of the 3D systems in the presence of high concentration of anions, the experimental part was adapted from [33], using a molar ratio of MOF to the salt containing the exchange anions of 1:15. A 1 mL suspension containing 20 mg of microcrystalline MOF (**1** or **2**, respectively) was added to 4 mL solutions of different salts, namely: NH$_4$PF$_6$, KNO$_3$, KMnO$_4$, K$_2$CrO$_4$, and KClO$_4$. The final solutions were then left for 10 days at room temperature and without any stirring, after which were analyzed by FTIR spectroscopy. The corresponding concentration of salt solution for this ratio is 58 mM.

The comparative FTIR spectra of **1** and **2** immersed in different anions solutions are presented in Figures II.3.1-8 and II.3.1-9, respectively. As it can be observed, no significant changes are present in the spectra, except in the case of MnO$_4{}^-$. For this solution the spectra is slightly modified which may be caused by a mild oxidation of the ligand to a vicinal diol.

This concludes that for the given conditions: room temperature, atmospheric pressure, no stirring and a high concentration of anions, no exchange occurred in these Cu-based coordination polymers when NO$_3{}^-$, PF$_6{}^-$, CrO$_4{}^{2-}$, or ClO$_4{}^-$ were investigated for anion-exchange, while in the presence of MnO$_4{}^-$ a chemical modification occurred.
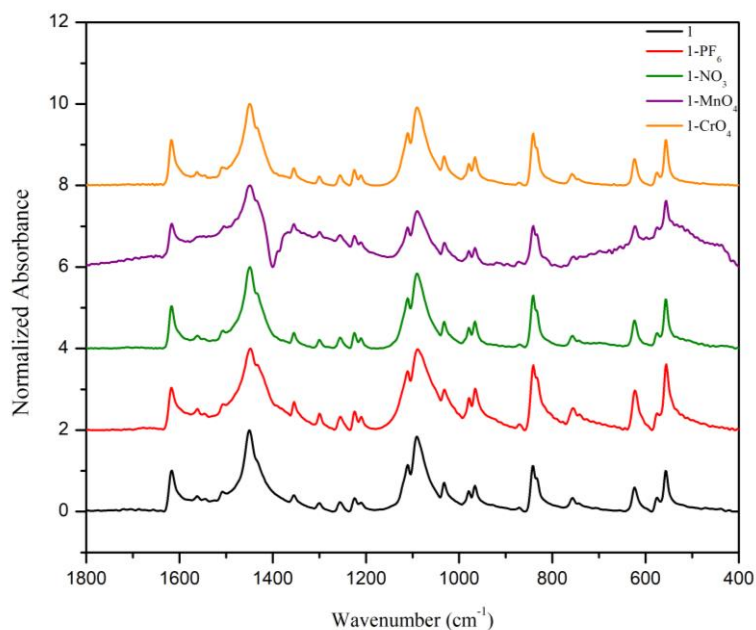
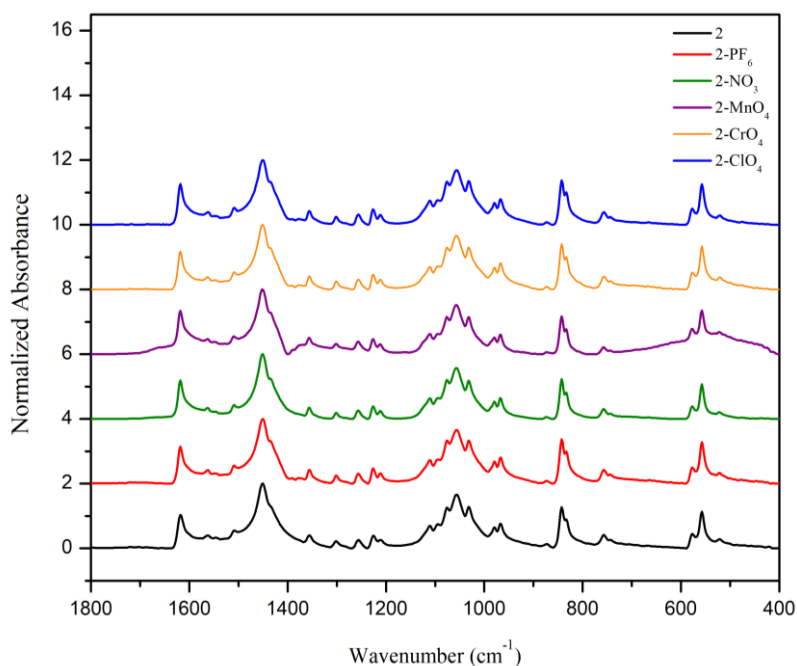**Fig.II.3.1-8.** FTIR spectra of **1** immersed in solutions of different anions

Fig.II.3.19. FTIR spectra of **2** immersed in solutions of different anions

II.3.2. Adsorption properties

The adsorption properties of the compounds were evaluated based on the nitrogen adsorption-desorption measurements performed at 77 K and a partial pressure (p/p_0) range of $10^{-3} - 1$ bar. Samples of each compound were degassed under vacuum $(< 10^{-2}$ mbar) at 150 °C for 3 – 18h prior to measurement in order to free the pores of any guest molecules.

In Figure II.3.2-1 are presented the N_2 adsorption-desorption isotherms on the obtained compounds. It can be observed that for compounds **1-4** the adsorbed volumes are in the range of $9 - 25$ cm^3/g while for **5** and **6** the adsorbed volumes are 400 cm^3/g and 150 cm^3/g, respectively. It had been noticed that higher uptakes are achieved in the case of the compounds containing the perchlorate anions.
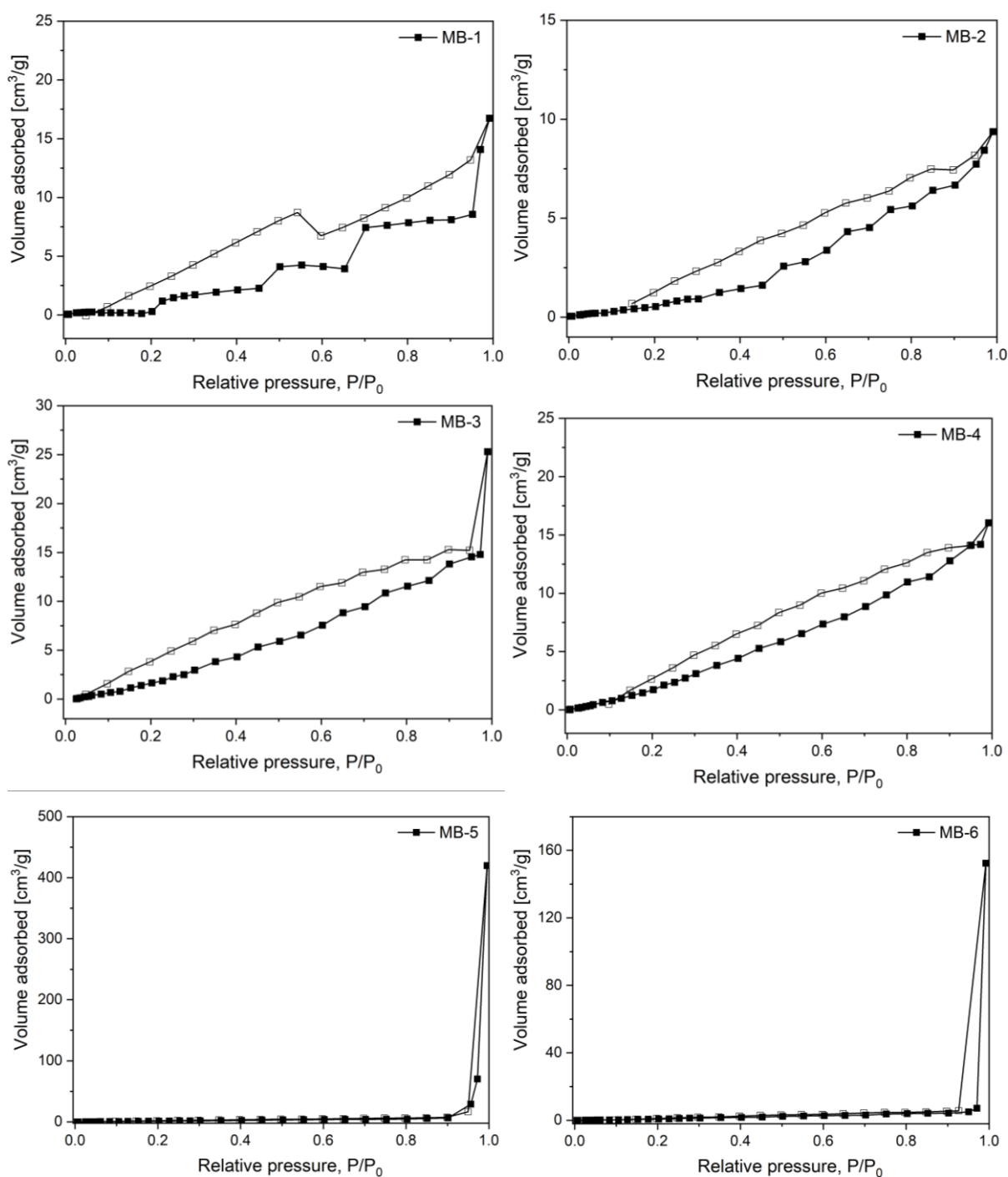

Fig.II.3.2-1. N_2 adsorption-desorption isotherms on compounds **1-6**

The adsorption isotherms of **1** and **2** are similar to a type VI isotherm combined with a H3 hysteresis loop. Usually, this type of isotherm describes a multilayer adsorption, but taking into account the structure of the synthesized compounds it would rather suggest a "breathing mechanism" with the steps associated to an expansion movement which allows a higher uptake as the relative pressure increases [40]. Compounds **3** and **4** exhibit a type III isotherm combined with a H3 hysteresis loop, which indicates a small adsorbed amount at low pressures, probably due to relatively weak interactions between the adsorbate and the adsorbent [41]. The higher adsorbed volume in the case of compounds **5** and **6** may be explained by an aggregation of the microcrytallites at high relative pressures ($p/p_0 = 0.9$) which provide a high surface area.

The N_2 adsorption measurements revealed that these compounds does not exhibit a high porosity, which is expected for MOFs, but at the same time confirm the existence of void space along the hexagonal channels. Powder X-ray diffractograms recorded before and after N_2 adsorption revealed that the crystallinity of the probes remain intact when exposed to pressure differences and are presented in Appendix (section D, Figures D.1 – D.6).

Conclusions

In the present dissertation thesis we have proposed the synthesis of Cu-based metal-organic frameworks capable of chemically fixing the atmospheric CO_2 into their structure and which, subsequently, will be able to allow its further capture by adsorption into the pores. The obtained compounds were characterized in solid state through single crystal and powder X-ray diffraction, along with spectroscopic techniques (FT-IR and UV-Vis), thermogravimetric analysis, and elemental analysis.

The single crystal XRD revealed the formation of 2D $Cu(CO_3)$ layers with a Kagomé arrangement, through direct fixation of atmospheric CO_2, which are further link via bipyridine-based ligands yielding to a 3D cationic framework with hybrid structure. All six compounds are isostructural and have the general formula $\{[Cu_3(CO_3)_2(L)_3](Y)_2\}_n$, where L = organic ligand and Y = ClO_4^- or BF_4^- anions. The influence of the organic linker on the interlayer distance is directly proportional to the length of the linker. The purity of the compounds was assessed based on the powder X-ray diffraction, which shown only one crystalline phase. The thermogravimetric analysis revealed a relatively high thermal stability for this class of compounds, approximately 300 °C, generated by the arrangement of the building blocks as well as the non-covalent interactions established across the entire structure: hydrogen bonds, electrostatic, and CH-π interactions.

Anion-exchange and adsorption properties of the obtained MOFs were investigated. Different salts were employed for the anion-exchange, and the process was monitored with spectroscopic techniques. The result concluded that no anion-exchange occurred at room temperature and atmospheric pressure, regardless of concentration of the anion solutions used. This may be explained by the fact that the anions are rather trapped within the structure and does not allow any exchange. When MnO_4^- anion was employed, with compounds **1** and **2,** a post-synthetic chemical transformation on the surface of the crystals was most probable taking place, namely a Bayer oxidation of the ethylene double bond.

Regarding the adsorption properties, the compounds do not exhibit a high porosity, as most of the space is occupied by the counter anions. However, the compounds maintain their structure at pressure variations. A higher uptake could be achieved by utilizing longer ligands and/or metals salts with smaller anions ($CuCl_2$, $Cu(NO_3)_2$, $Cu(CN)_2$) or by recrystallizing the compounds from a salt solution that has smaller anions.

In the future, we aim to fully investigate the adsorption capacity of the synthesized compounds for water vapors, carbon dioxide and volatile organic compounds.

Acknowledgements

Materials and Instrumentation

Reagents and solvents

The reagents used in this study were: 1,2-bis(4-pyridyl)ethane (bpe), 1,2-bis(4-pyridyl)ethylene (bpy), 4,4'-azopyridine (azopy), Copper(II) tetrafluoroborate hexahydrate ($Cu(BF_4)_2 \cdot 6H_2O$), Copper(II) perchlorate hexahydrate ($Cu(ClO_4)_2 \cdot 6H_2O$), and aqueous ammonia (NH_4OH, 25%), ammonium hexafluorophosphate (NH_4PF_6), potassium nitrate (KNO_3), potassium permanganate ($KMnO_4$), potassium chromate (K_2CrO_4), and potassium perchlorate ($KClO_4$). All reagents were procured from Sigma-Aldrich and used without any further purification. The solvents used were methanol (CH_3OH) and distilled water (obtained in the laboratory).

Instrumentation

Weighing: Reagents and synthesized compounds were weighed on the analytical balance *Mettler Toledo XS204/M* with 5 decimal places.

Spectral determinations:

The infrared spectra were recorded in the $4000 - 400$ cm^{-1} range by the Fourier Transformer *Tensor 27* Spectrometer (FT-IR) using OPUS software. The processing of the samples consisted in preparation of pellets from a pre-ground mixture of sample with KBr using *Grasebz Spec 15011* press. The graphical representations were realized with Origin 8.5 software.

The UV-Vis spectra were recorded on solid and on solution in the 200 – 850 nm range with the help of a *JASCO V-670* spectrophotometer and with the use of Spectra Manager software. The graphical representations were prepared with Origin 8.5 software.

X-ray diffraction:

Single crystal X-ray diffraction measurements were carried out using a *Rigaku XtaLAB Synergy-S* diffractometer operating with Mo-Kα ($\lambda = 0.71073$ Å) micro-focus sealed X-ray tube. Calculations were performed using *ShelX* crystallographic software and the representations were achieved with the help of the *Diamond 3.2*.

The X-ray powder diffraction measurements (PXRD) were carried out on a *Proto AXRD Benchtop* using the Cu-Kα radiation with a wavelength of 1.54059 Å in the 5 - 35º range of *2θ*. The graphical representations were performed with Origin 8.5 software.

PXRD data before and after the nitrogen physisorption isotherms were collected at room temperature on *Rigaku Miniflex 600* powder diffractometer (Germany) using Cu-Kα radiation ($\lambda = 1.5418$ Å) between $2° < 2\theta < 50°$ with a scanning rate of 1.5 deg/min (600 W, 40 kV, 15 mA). Analyses of the diffractograms were carried out with Origin 8.5 software.

Elemental analysis:

The elemental analysis was performed on a *Euro EA Elemental Analyzer* and the collected data were integrated with Callidus 4.1 software.

TGA:

Thermogravimetric analysis (TGA) was performed on a *Netzsch TG209 F3 Tarsus (Netzsch, Selb, Germany)* device under nitrogen conditions, ramping with 10 K/min from 30 °C to 600 °C.

N$_2$ physisorption:

The nitrogen (purity 99.9990%) physisorption isotherms were carried out at 77 K using a *Quantachrome Autosorb 6* instrument within a partial pressure range of $p/p_0 = 10^{-3}$–1 bar. Each sample of ca. 30 mg was degassed under vacuum ($< 10^{-2}$ mbar) at 150 °C for 3 – 18 h prior to measurement.

References

1. United States Environmental Protection Agency (EPA), website: https://www.epa.gov/ghgemissions/global-greenhouse-gas-emissions-data

2. Friedlingstein, P., O'Sullivan, M., Jones, M.W., Andrew, R.M., Hauck, J., Olsen, A., Peters, G.P., Peters, W., Pongratz, J., Sitch, S., Le Quéré, C., Canadell, J.G., Ciais, P., Jackson, R.B., Alin, S., Aragão, L.E.O.C., Arneth, A., Arora, V., Bates, N.R., Becker, M., Benoit-Cattin, A., Bittig, H.C., Bopp, L., Bultan, S., Chandra, N., Chevallier, F., Chini, L.P., Evans, W., Florentie, L., Forster, P.M., Gasser, T., Gehlen, M., Gilfillan, D., Gkritzalis, T., Gregor, L., Gruber, N., Harris, I., Hartung, K., Haverd, V., Houghton, R,A., Ilyina, T., Jain, A.K., Joetzjer, E., Kadono, K., Kato, E., Kitidis, V., Korsbakken, J.I., Landschützer, P., Lefèvre, N., Lenton, A., Lienert, S., Liu, Z., Lombardozzi, D., Marland, G., Metzl, N., Munro, D.R., Nabel, J.E.M.S., Nakaoka, S.-I., Niwa, Y., O'Brien, K., Ono, T., Palmer, P.I., Pierrot, D., Poulter, B., Resplandy, L., Robertson, E., Rödenbeck, C., Schwinger, J., Séférian, R., Skjelvan, I., Smith, A.J.P., Sutton, A.J., Tanhua, T., Tans, P.P., Tian, H., Tilbrook, B., van der Werf, G., Vuichard, N., Walker, A.P., Wanninkhof, R., Watson, A.J., Willis, D., Wiltshire, A.J., Yuan, W., Yue, X., Zaehle, S., Global Carbon Budget 2020, Earth Syst. Sci. Data, 12 (4) (2020), 3269:3340.

3. Oelkers, E.H., Cole, D.R., Carbon Dioxide Sequestration A Solution to a Global Problem. Elements, 4(5) (2008), 305:310.

4. Tamilselvi Dananjayan, R.R., Kandasamy, P., Andimuthu, R., Direct mineral carbonation of coal fly ash for CO_2 sequestration. J. Clean. Prod., 112 (2016), 4173:4182.

5. Verma, R., Srivastava, A., Carbon dioxide sequestration and its enhanced utilization by photoautotroph microalgae. Environ. Dev., 27 (2018), 95:106.

6. Keene, T.D., Murphy, M.J., Price, J.R., Sciortino, N.F., Southon, P.D., Kepert, C.J., Multifunctional MOFs through CO_2 fixation: a metamagnetic kagome lattice with uniaxial zero thermal expansion and reversible guest sorption. Dalton Trans., 43(39) (2014), 14766:14771.

7. Zhou, H.-C., Long, J.R., Yaghi, O.M., Introduction to Metal–Organic Frameworks. Chem. Rev., 112(2) (2012), 673:674.

8. Bu, F.-X., Hu, M., Xu, L., Meng, Q., Mao, G.-Y., Jiang, D.-M., Jiang, J.-S., Coordination polymers for catalysis: enhancement of catalytic activity through hierarchical structuring. Chem. Commun., 50(62) (2014), 8543:8546.

9. Bon, V., Senkovska, I., Kaskel, S., Nanoporous Materials for Gas Storage, Green Energy and Technology, Ed. Springer, Singapore, 2019, Chapter 6: Metal-Organic Frameworks, pgs. 137-172.

10. Janiak, C., Vieth, J.K., MOFs, MILs and more: concepts, properties and applications for porous coordination networks (PCNs). New J. Chem., 34(11) (2010), 2366-2388.

11. Mashhadzadeh, A.H., Taghizadeh, A., Taghizadeh, M., Munir, M.T., Habibzadeh, S., Salmankhani, A., Stadler, F.J., Saeb, M.R., Metal-Organic Framework (MOF) through the Lens of Molecular Dynamics Simulation: Current Status and Future Perspective. J. Compos. Sci., 4(2) (2020), 75:88.

12. Seo, J., Sakamoto, H., Matsuda, R., Kitagawa, S., Chemistry of Porous Coordination Polymers Having Multimodal Nanospace and Their Multimodal Functionality. J. Nanosci. Nanotechnol., 10(1) (2010), 3:20.

13. Sánchez-Serratos, M., Álvarez, J.R., González-Zamora, E., Ibarra, I.A., Porous Coordination Polymers (PCPs): New Platforms for Gas Storage. J. Mex. Chem. Soc., 60(2) (2016), 43:57.

14. Robin, A.Y., Fromm, K.M., Coordination polymer networks with O- and N-donors: What they are, why and how they are made. Coord. Chem. Rev., 250(15-16) (2006), 2127:2157.

15. Khandar, A.A., Afkhami, F.A., Hosseini-Yazdi, S.A., White, J.M., Kassel, S., Dougherty, W.G., Lipkowski, J., Van Derveer, D., Giester, G., Costantino, F., Anion influence in the structural diversity of cadmium coordination polymers constructed from a pyridine based Schiff base ligand. Inorg. Chim. Acta, 427 (2015), 87:96.

16. Liu, J.-J., Xia, S.-B., Duan, Y.-L., Liu, T., Cheng, F.-X., Sun, C.-K., Anion-Controlled Architecture and Photochromism of Naphthalene Diimide-Based Coordination Polymers. Polymers, 10(2) (2018), 165:176.

17. Ghosh, A., Hazra, A., Mondal, A., Banerjee, P., Weak interactions: the architect behind the structural diversity of coordination polymer. Inorg. Chim. Acta, 488 (2019), 86:119.

18. Hönicke, I., Senkovska, I., Bon, V., Baburin, I., Boenisch, N., Raschke, S., Kaskel, S., Balancing Mechanical Stability and Ultrahigh Porosity in Crystalline Framework Materials, Angew. Chem. Int. Ed., 57(42) (2018), 13780:13783

19. Bureekaew, S., Shimomura, S., Kitagawa, S., Chemistry and application of flexible porous coordination polymers, Sci. Technol. Adv. Mater., 9(1) (2008), 014108:014119.

20. Hasegawa, S., Horike, S., Matsuda, R., Furukawa, S., Mochizuki, K., Kinoshita, Y., Kitagawa, S., Three-Dimensional Porous Coordination Polymer Functionalized with

Amide Groups Based on Tridentate Ligand: Selective Sorption and Catalysis. J. Am. Chem. Soc., 129(9) (2007), 2607:2614.

21. El-Shall, M.S., Abdelsayed, V., Khder, A.E.R.S., Hassan, H.M.A., El-Kaderi, H.M., Reich, T.E., Metallic and bimetallic nanocatalysts incorporated into highly porous coordination polymer MIL-101. J. Mater. Chem., 19(41) (2009), 7625:7631.

22. Kong, X., Deng, H., Yan, F., Kim, J., Swisher, J.A., Smit, B., Yaghi, O.M., Reimer, J.A., Mapping of Functional Groups in Metal-Organic Frameworks. Science, 341(6148) (2013), 882:885.

23. Chen, D., Liang, F., Feng, D., Xian, M., Zhang, H., Liu, H., Du, F., An efficient route from reproducible glucose to 5-hydroxymethylfurfural catalyzed by porous coordination polymer heterogeneous catalysts. Chem. Eng. J., 300 (2016), 177:184.

24. Peedikakkal A.M.P., Adarsh N.N., Porous Coordination Polymers in Jafar Mazumder M., Sheardown H., Al-Ahmed A. (eds) Functional Polymers. Polymers and Polymeric Composites: A Reference Series. Springer, Cham (2019).

25. Li, H., Wang, K., Sun, Y., Lollar, C.T., Li, J., Zhou, H.-C., Recent advances in gas storage and separation using metal–organic frameworks. Mater. Today, 21(2) (2018), 108:121.

26. De, D., Pal, T.K., Neogi, S., Senthilkumar, S., Das, D., Gupta, S.S., Bharadwaj, P.K., A Versatile Cu^{II} Metal-Organic Framework Exhibiting High Gas Storage Capacity with Selectivity for CO_2: Conversion of CO_2 to Cyclic Carbonate and Other Catalytic Abilities. Chem.: Eur. J., 22(10) (2016), 3387:3396.

27. Saha, D., Deng, S., Hydrogen adsorption on metal-organic framework MOF-177. Tsinghua Sci. Technol., 15(4) (2010), 363:376.

28. He, Y., Chen, F., Li, B., Qian, G., Zhou, W., Chen, B., Porous metal–organic frameworks for fuel storage. Coord. Chem. Rev., 373 (2018), 167:198.

29. Jiang, J., Furukawa, H., Zhang, Y.-B., Yaghi, O.M., High Methane Storage Working Capacity in Metal–Organic Frameworks with Acrylate Links. J. Am. Chem. Soc., 138(32) (2016), 10244:10251.

30. Leroux, M., Mercier, N., Allain, M., Dul, M.-C., Dittmer, J., Kassiba, A.H., Bezverkhyy, I., Porous Coordination Polymer Based on Bipyridinium Carboxylate Linkers with High and Reversible Ammonia Uptake. Inorg. Chem., 55(17) (2016), 8587:8594.

31. Belmabkhout, Y., Pillai, R.S., Alezi, D., Shekhah, O., Bhatt, P.M., Chen, Z., Eddaoudi, M., Metal–organic frameworks to satisfy gas upgrading demands: fine-tuning the soc-

MOF platform for the operative removal of H$_2$S. J. Mater. Chem. A, 5(7) (2017), 3293:3303.

32. Kumar, P., Pournara, A., Kim, K.-H., Bansal, V., Rapti, S., Manos, M.J., Metal-organic frameworks: Challenges and opportunities for ion-exchange/sorption applications. Prog. Mater. Sci., 86 (2017), 25:74.

33. Phuengphai, P., Massera, C., Reedijk, J., Youngme, S., Gamez, P., Anion Exchange in Coordination-Network Materials. Eur. J. Inorg. Chem., 2013(27) (2013), 4812:4822.

34. Noori, Y., Akhbari, K., Post-synthetic ion-exchange process in nanoporous metal–organic frameworks; an effective way for modulating their structures and properties. RSC Adv., 7(4) (2017), 1782:1808.

35. Nakamoto, K., Infrared and Raman Spectra of Inorganic and Coordination Compounds; John Wiley and Sons: New Jersey, USA, (2009).

36. Asadi, H.; Golchoubian, H., Synthesis, structural and solvent influence studies on solvatochromic of acetylacetonatocopper(II) with N,N' -dibenzylic or thiophene derivatives of ethylenediamine complexes. J. Mol. Struct., 779 (2005), 30:37.

37. Lever, A.B.P., Inorganic Electronic Spectroscopy (2nd Edition), Elsevier, 1984.

38. Hoskins, B.F., Robson, R., Design and construction of a new class of scaffolding-like materials comprising infinite polymeric frameworks of 3D-linked molecular rods. A reappraisal of the zinc cyanide and cadmium cyanide structures and the synthesis and structure of the diamond-related frameworks [N(CH$_3$)$_4$][Cu^{I}Zn^{II}(CN)$_4$] and Cu^I[4,4',4'',4'''-tetracyanotetraphenylmethane]BF$_4$·xC$_6$H$_5$NO$_2$. J. Am. Chem. Soc., 112(4) (1990) 1546:1554.

39. Fernando, M.-P., Perez-Benito, J.F., Identification of the product from the reduction of permanganate ion by trimethylamine in aqueous phosphate buffers. Can. J. Chem., 63(4) (1985), 988:992.

40. Bourrelly, S., Llewellyn, P.L., Serre, C., Millange, F., Loiseau, T., Férey, G., Different Adsorption Behaviors of Methane and Carbon Dioxide in the Isotypic Nanoporous Metal Terephthalates MIL-53 and MIL-47. J. Am. Chem. Soc., 127(39) (2005), 13519:13521.

41. Cychosz, K.A., Guillet-Nicolas, R., García-Martínez, J., Thommes, M., Recent advances in the textural characterization of hierarchically structured nanoporous materials. Chem. Soc. Rev., 46 (2016),389:414.

Appendix

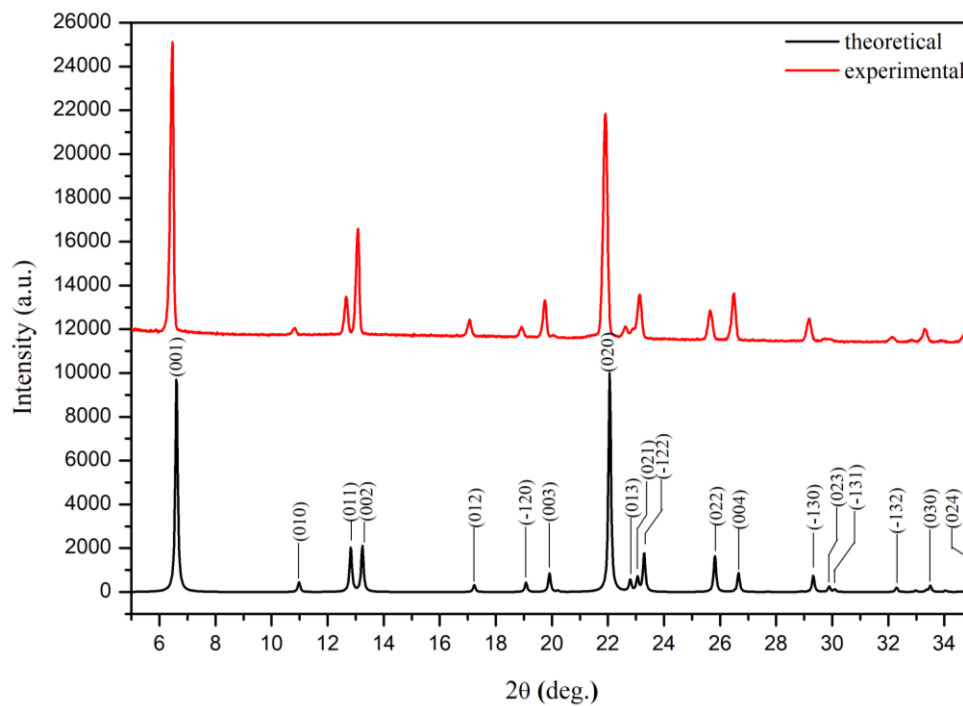**A. Powder X-ray diffractograms of compounds 1, 3-6**

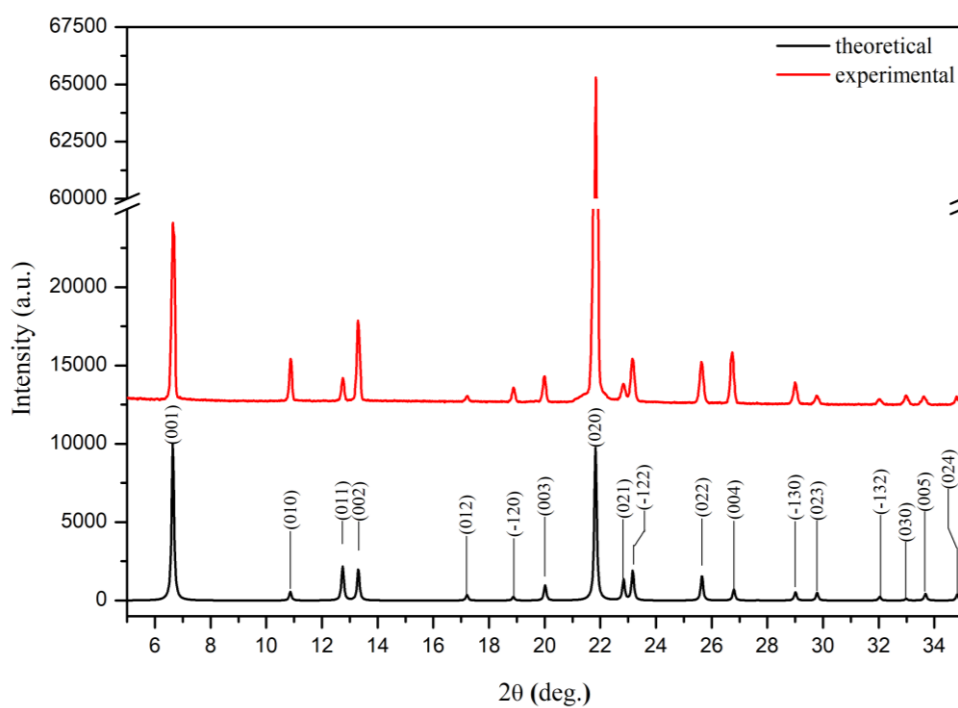**Fig.A1.** Powder XRD pattern of compound **1**
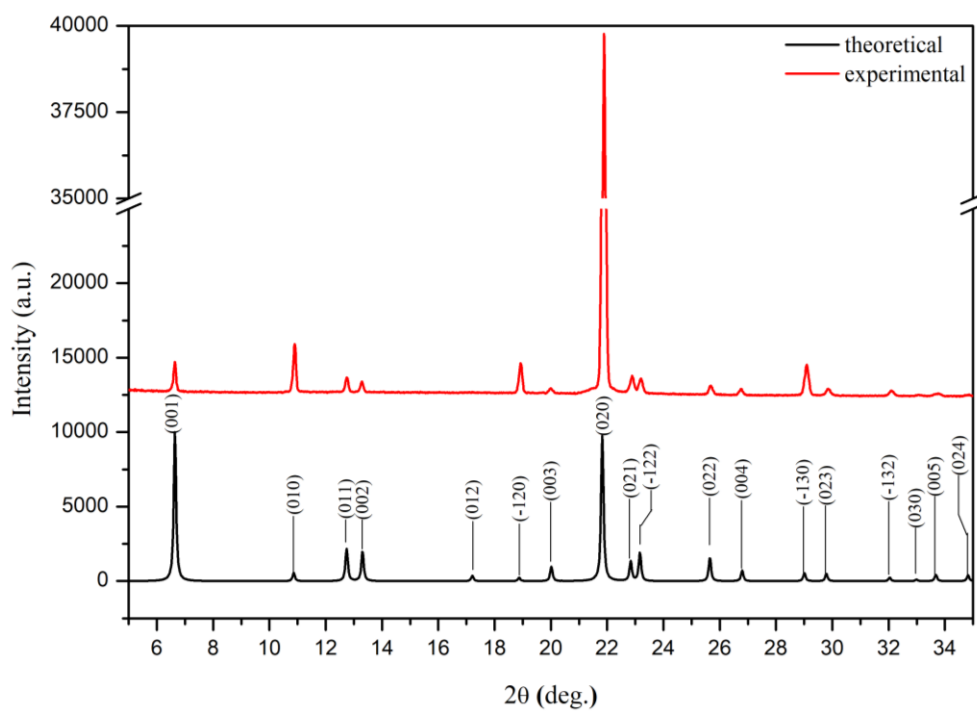

Fig.A2. Powder XRD pattern of compound **3**

Fig.A3. Powder XRD pattern of compound **4**
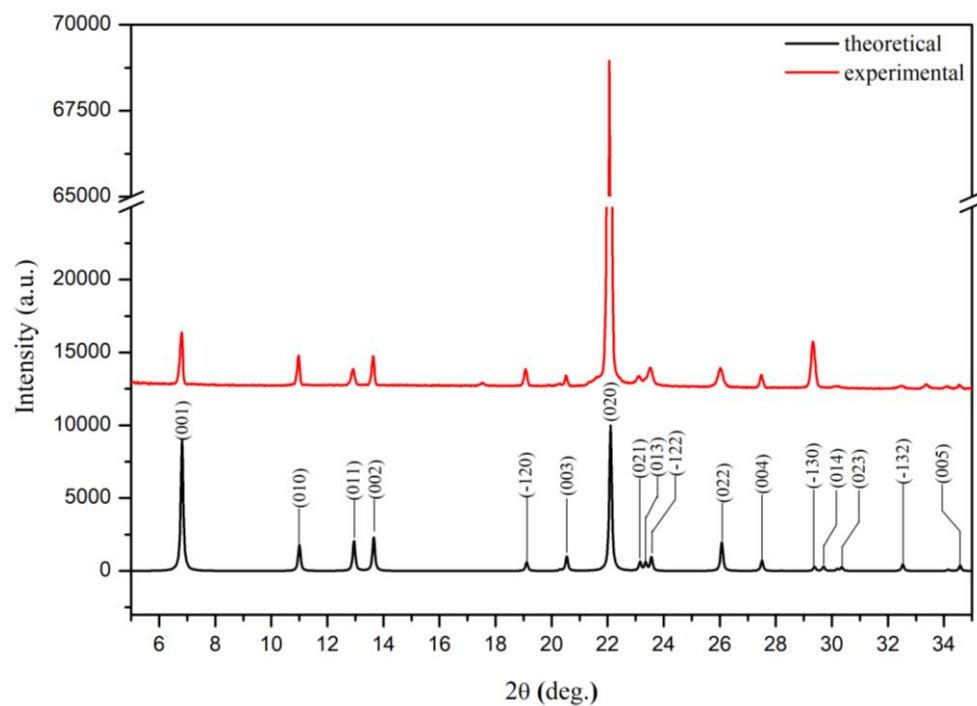
Fig.A4. Powder XRD pattern of compound **5**
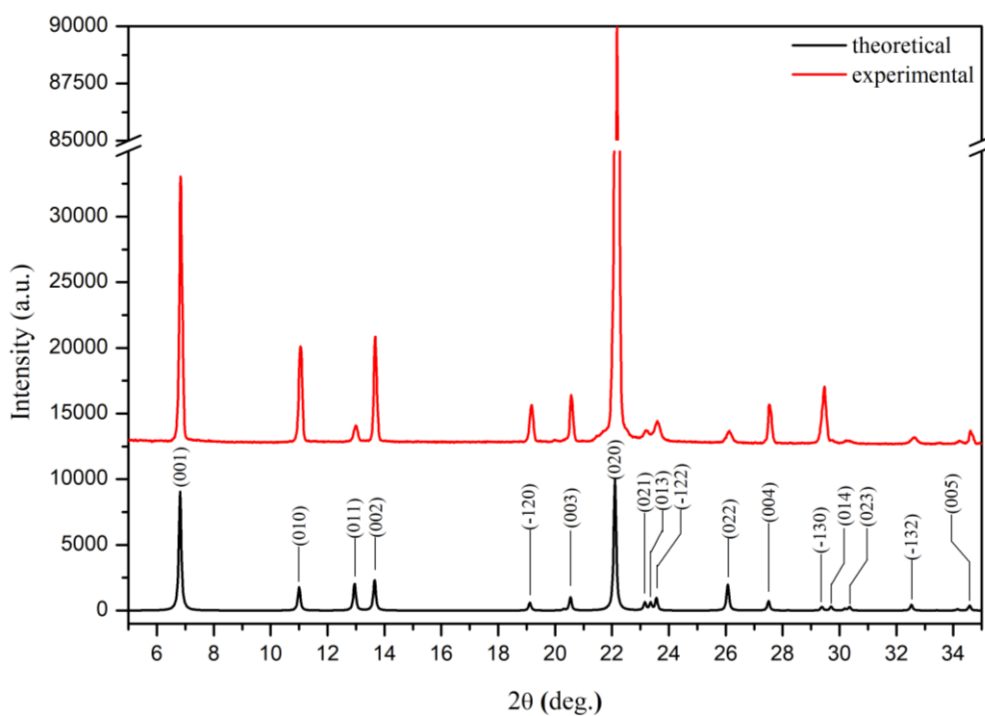
Fig.A5. Powder XRD pattern of compound **6**

B. Elemental analysis

Compound		% C	% N	% H
1	calculated	43.21	7.95	2.86
	found	42.41	7.87	2.79
2	calculated	44.27	8.15	2.93
	found	44.08	8.44	2.58
3	calculated	42.96	7.91	3.41
	found	42.40	7.99	3.40
4	calculated	44.01	8.10	3.50
	found	45.27	8.37	3.39
5	calculated	36.18	15.82	2.27
	found	36.26	15.66	2.21
6	calculated	37.06	16.21	2.33
	found	37.76	15.91	2.27

C. FTIR spectra of compounds 1-6
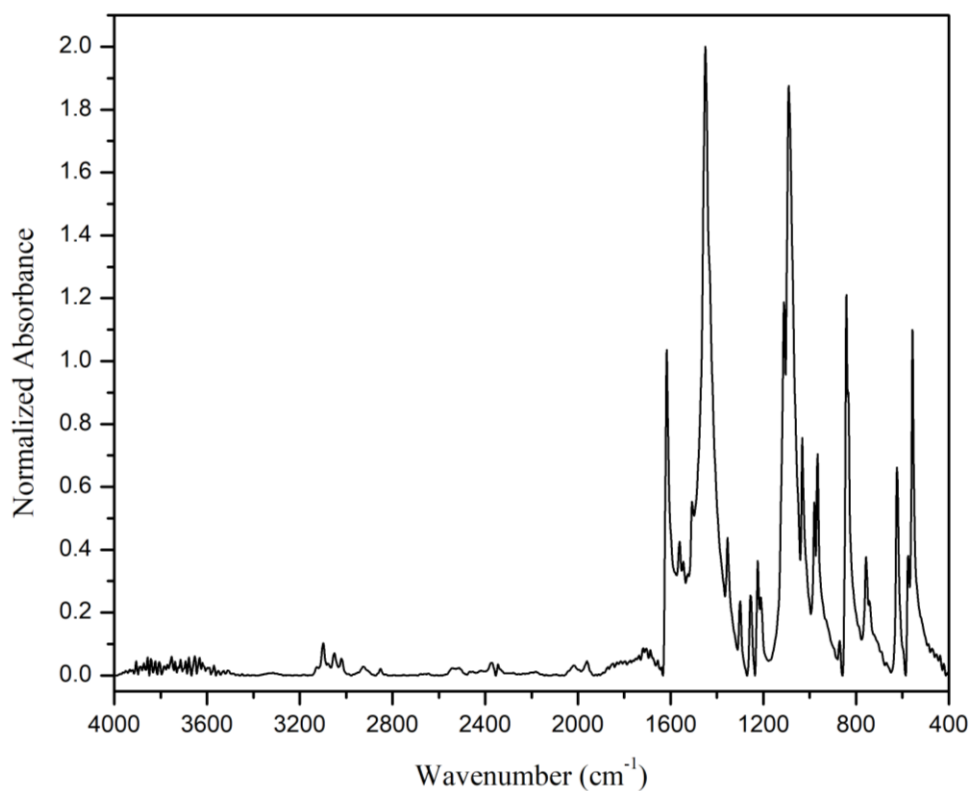
Fig.C1. FTIR spectrum of compound **1**
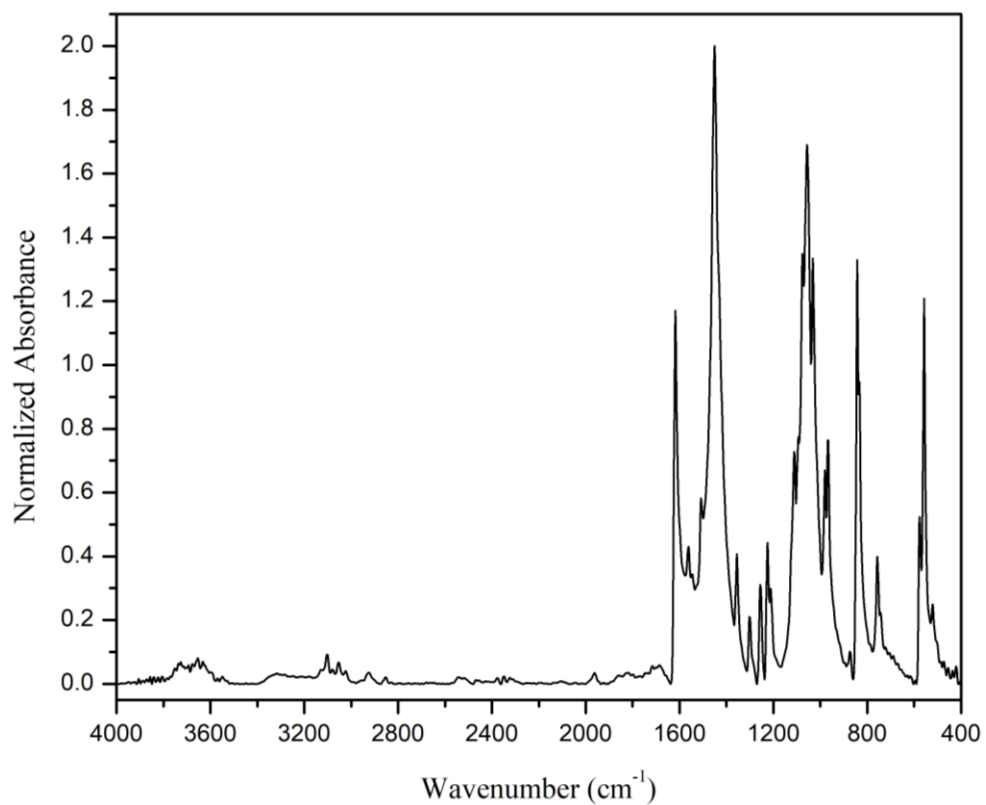
Fig.C2. FTIR spectrum of compound **2**
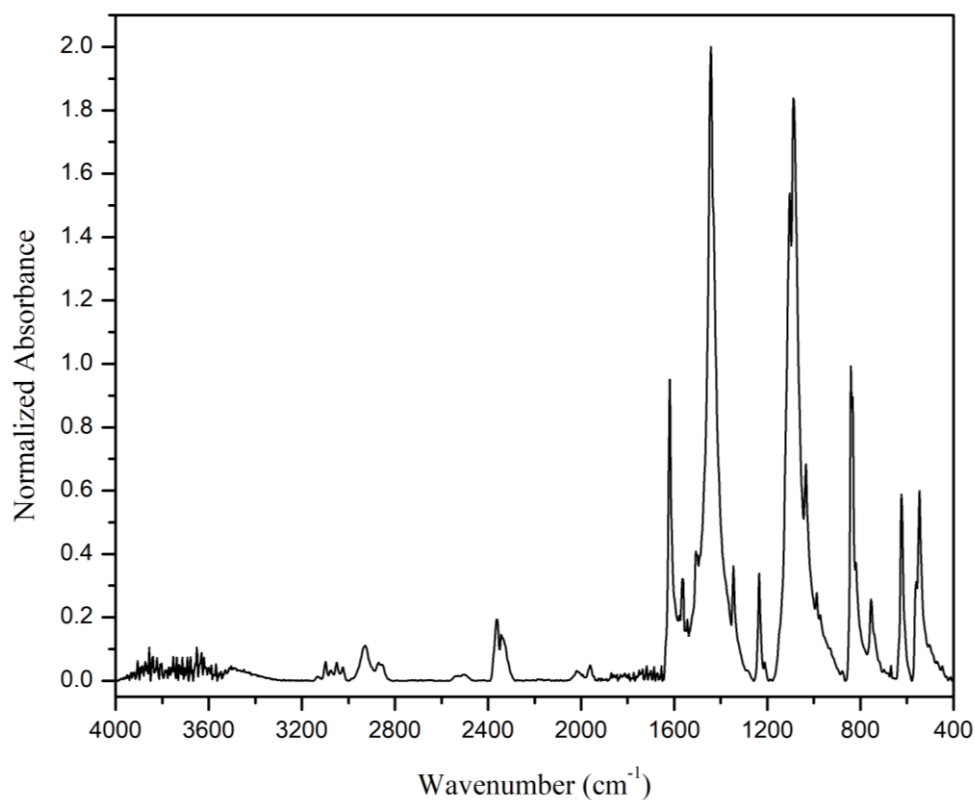
Fig.C3. FTIR spectrum of compound **3**
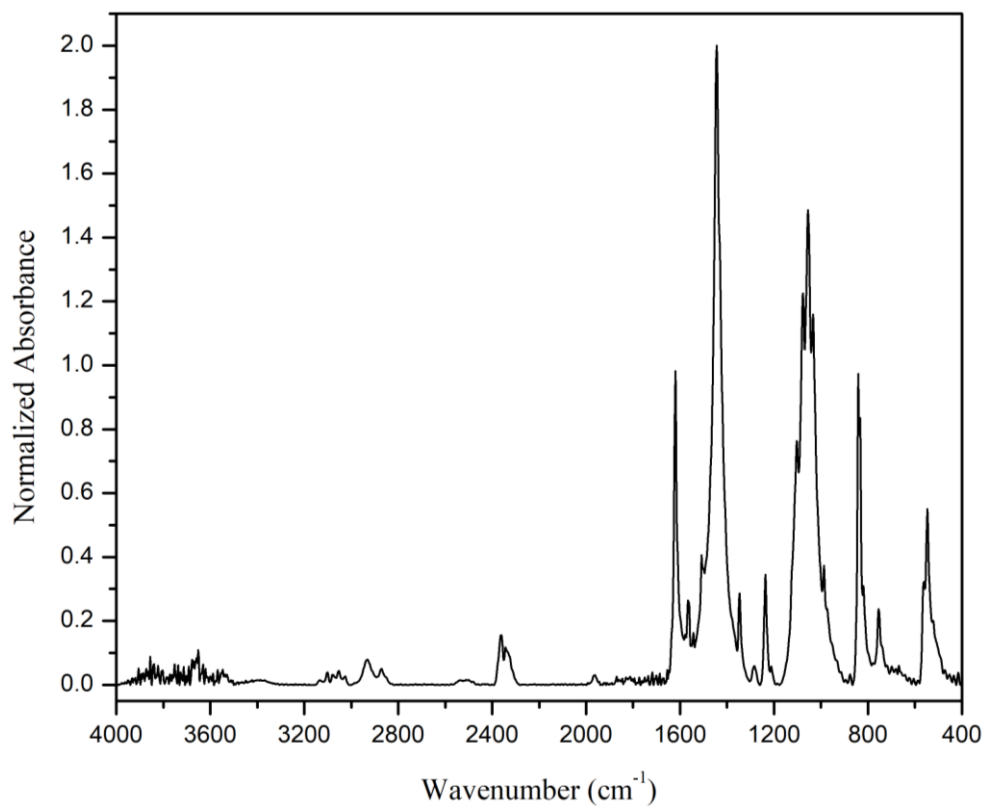
Fig.C4. FTIR spectrum of compound **4**
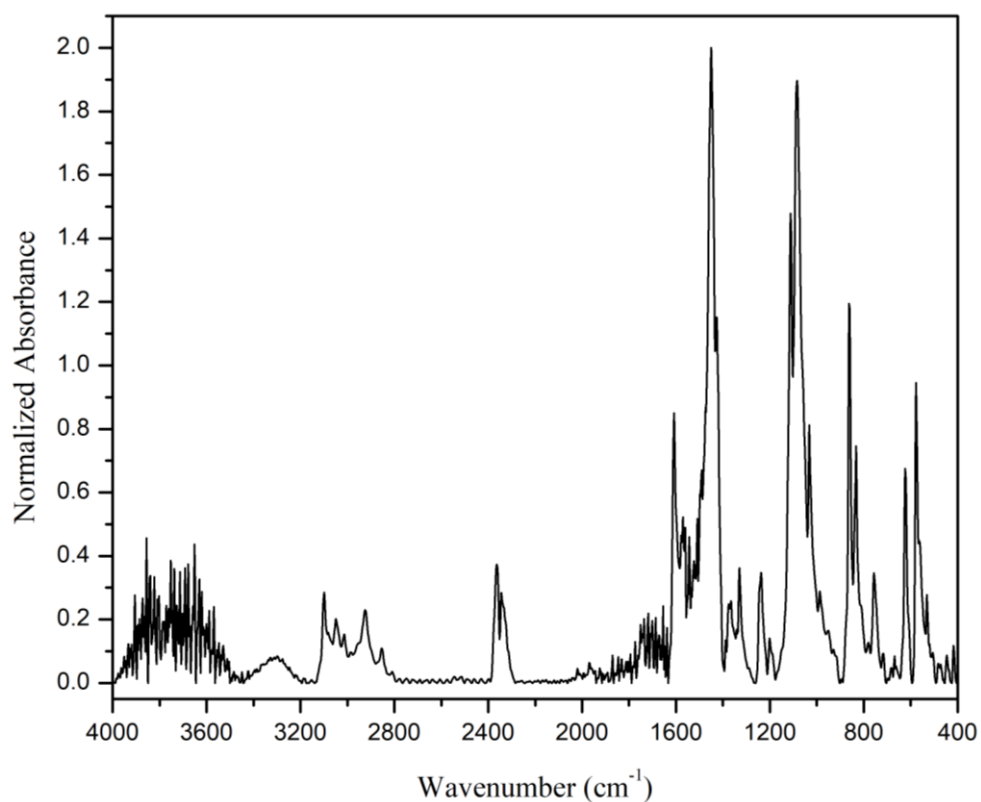
Fig.C5. FTIR spectrum of compound **5**
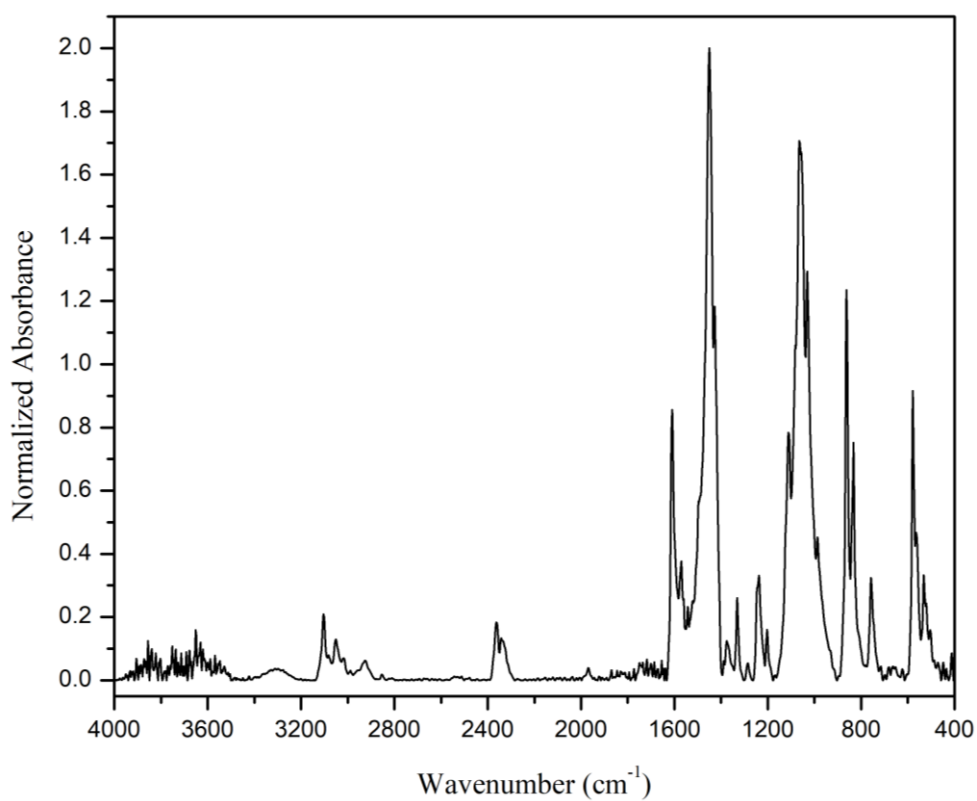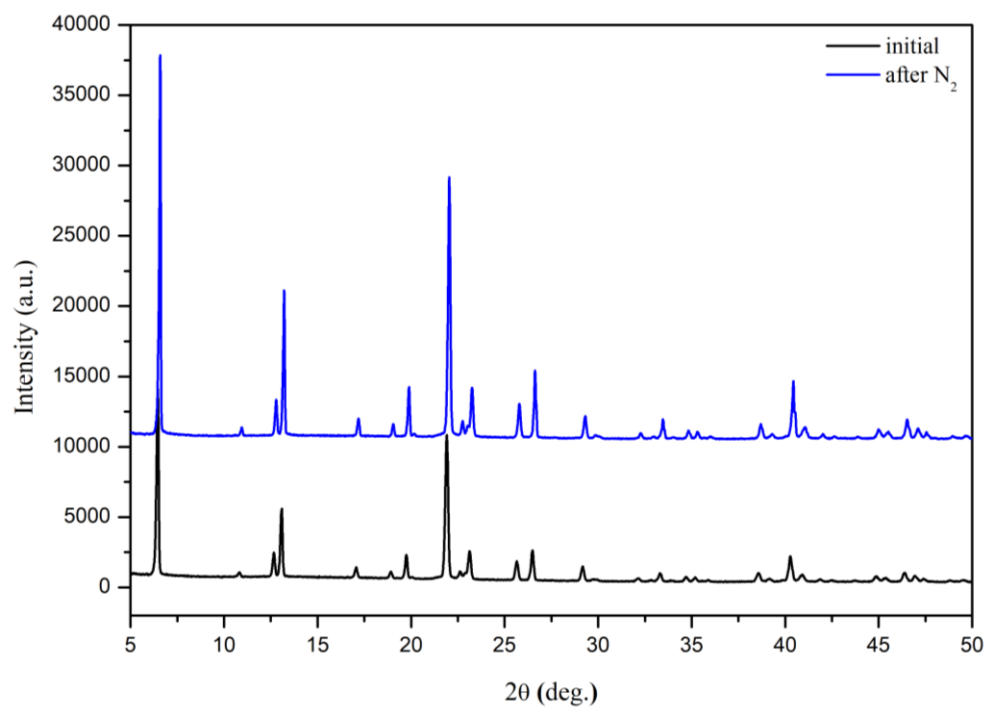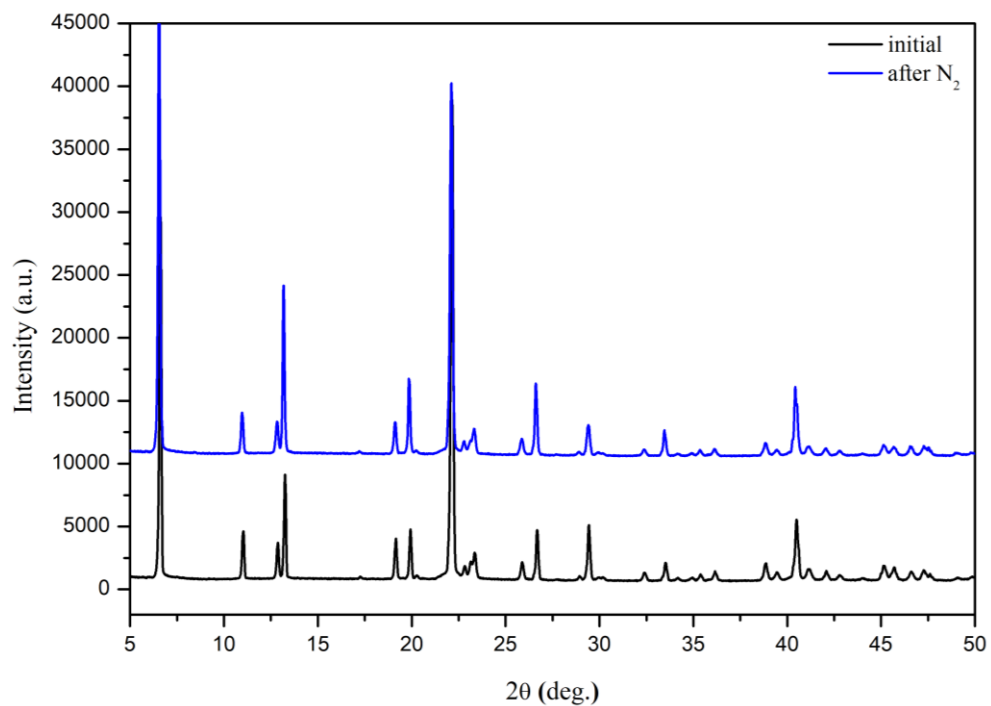

Fig.C6. FTIR spectrum of compound **6**

D. Powder X-ray diffractograms after N₂ sorption

Fig.D1. Powder XRD pattern of compound **1** before (black line) and after (blue line) N₂ sorption

Fig.D2. Powder XRD pattern of compound **2** before (black line) and after (blue line) N₂ sorption
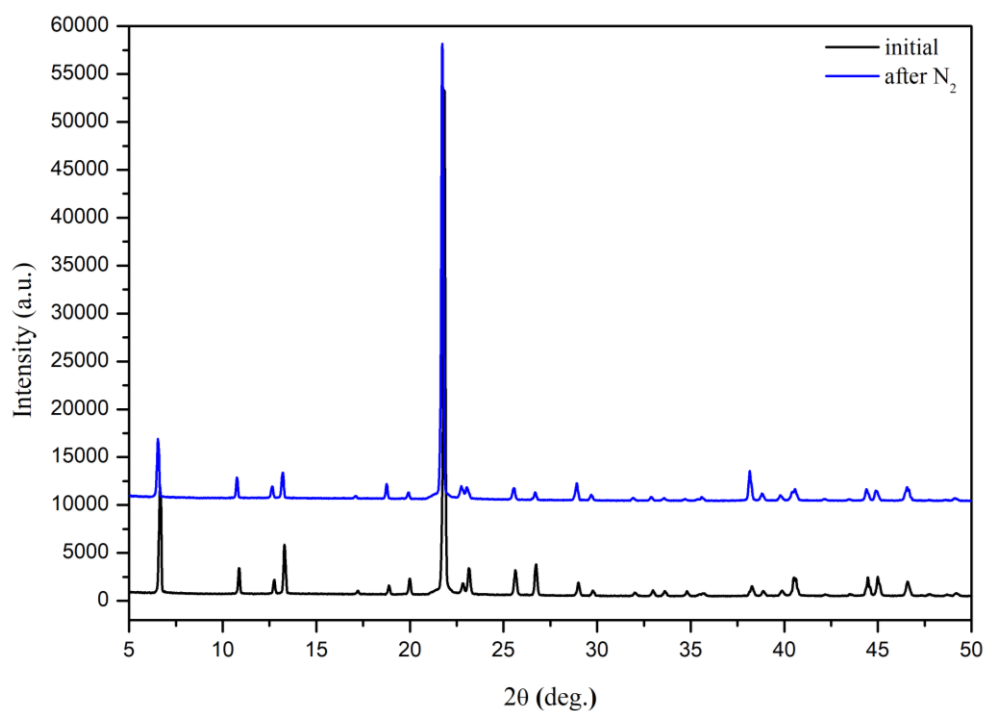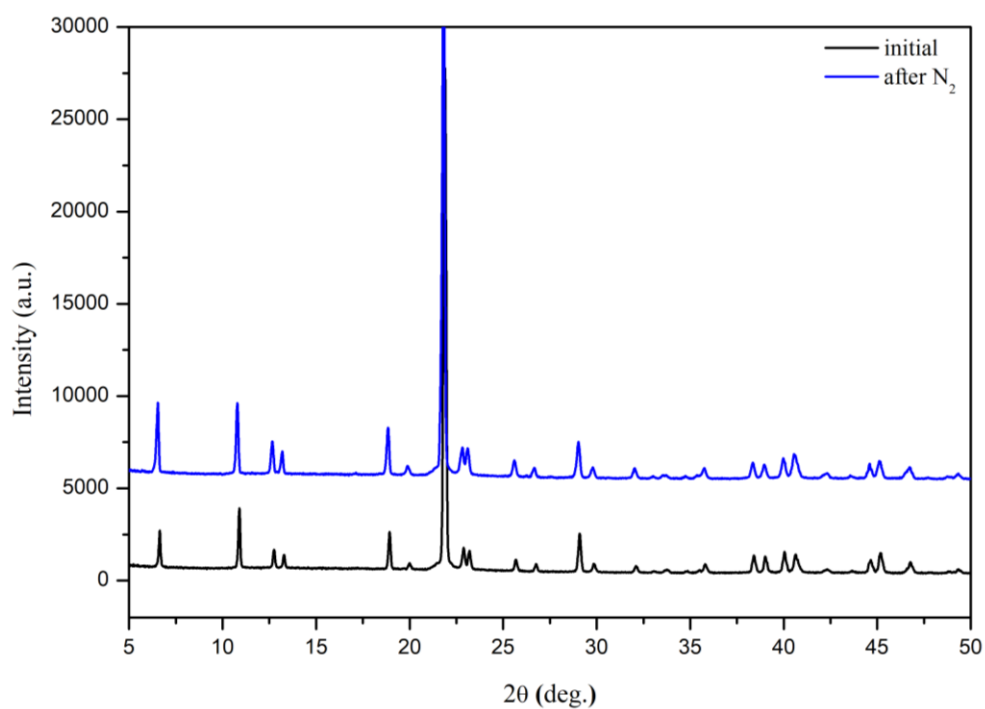
Fig.D3. Powder XRD pattern of compound **3** before (black line) and after (blue line) N_2 sorption

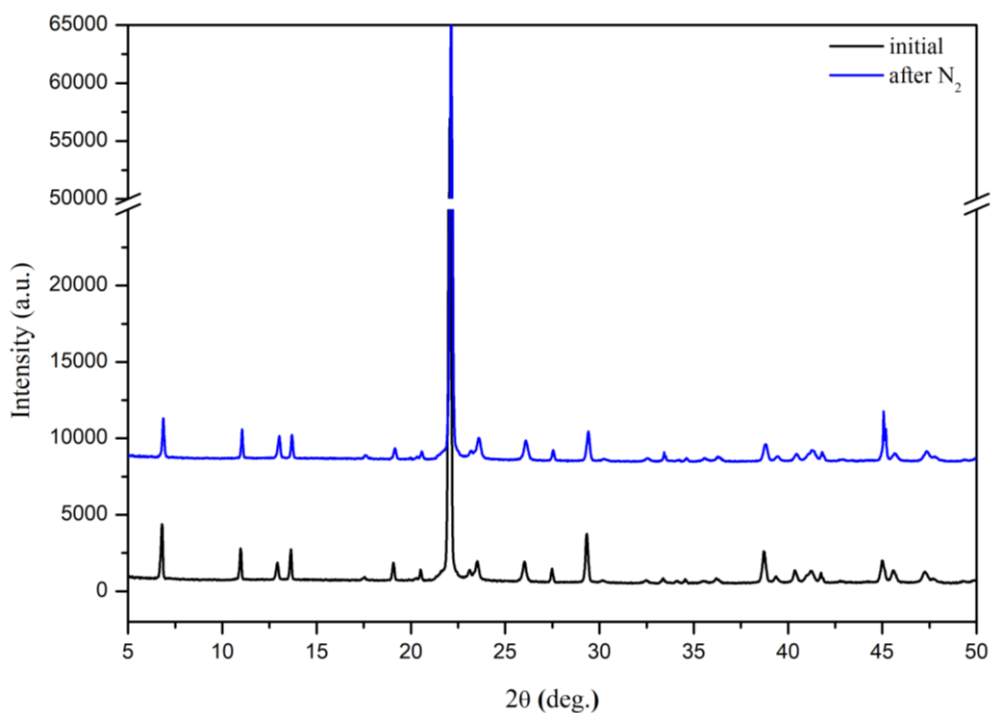**Fig.D4.** Powder XRD pattern of compound **4** before (black line) and after (blue line) N_2 sorption

Fig.D5. Powder XRD pattern of compound **5** before (black line) and after (blue line) N$_2$ sorption
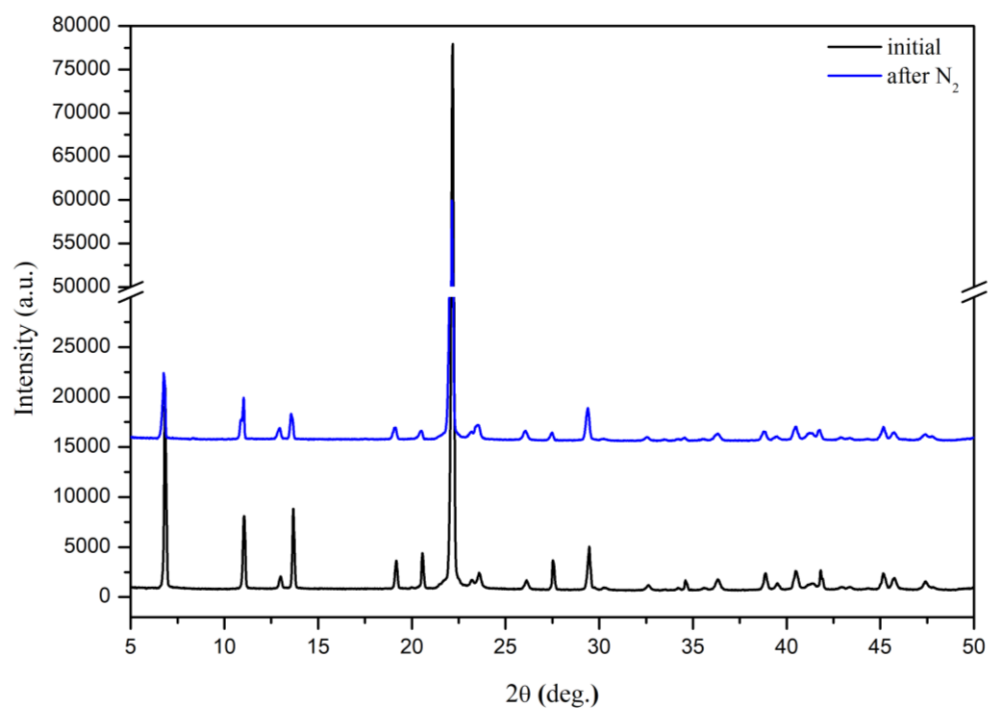

Fig.D6. Powder XRD pattern of compound **6** before (black line) and after (blue line) N$_2$ sorption